1 **Global patterns of surface ocean dissolved organic matter stoichiometry**

2

3 Zhou Liang[1*], Robert T. Letscher[2], and Angela N. Knapp[1]

4

5 [1]Department of Earth, Ocean and Atmospheric Science, Florida State University, Tallahassee,

6 FL, 32306

7 [2]Earth Sciences & Ocean Process Analysis Laboratory, University of New Hampshire,

8 Durham, NH, 03824

9

10 *Corresponding author: Zhou Liang (zl18c@fsu.edu)

11

12 **Key points**

13 • Surface ocean bulk and labile DOM stoichiometry vary across ocean regions with global

14 means of 387:26:1 and 179:20:1, respectively.

15

16 • The stoichiometries of bulk and labile surface ocean DON:DOP and DOC:DOP vary

17 more than DOC:DON due to variability in DOP concentrations.

18
19

20 • Surface ocean gradients in P-depleted DOM stoichiometries in the Pacific and Atlantic

21 basins reflect variable nutrient stress.

22

23 Keywords: dissolved organic matter, dissolved organic nitrogen, dissolved organic phosphorus,

24 stoichiometry

25

26

Abstract

Surface ocean marine dissolved organic matter (DOM) serves as an important reservoir of carbon (C), nitrogen (N), and phosphorus (P) in the global ocean, and is produced and consumed by both autotrophic and heterotrophic communities. While prior work has described distributions of dissolved organic carbon (DOC) and nitrogen (DON) concentrations, our understanding of DOC:DON:DOP stoichiometry in the global surface ocean has been limited by the availability of DOP concentration measurements. Here we estimate mean surface ocean bulk and labile DOC:DON:DOP stoichiometry in biogeochemically and geographically defined regions, using newly available marine DOM concentration databases. Global mean surface ocean bulk (C:N:P = 387:26:1) and labile (C:N:P = 179:20:1) DOM stoichiometries are higher than Redfield stoichiometry, with labile DOM stoichiometry similar to that of global mean surface ocean particulate organic matter (C:N:P = 160:21:1) reported in a recent compilation. DOM stoichiometry varies across ocean basins, ranging from 251:17:1 to 638:43:1 for bulk and 83:15:1 to 414:49:1 for labile DOM C:N:P, respectively. Surface ocean DOP exhibits larger relative changes than DOC and DON, driving surface ocean gradients in DOC:DON:DOP stoichiometry. Inferred autotrophic consumption of DOP helps explain intra- and inter-basin patterns of marine DOM C:N:P stoichiometry, with regional patterns of water column denitrification and iron supply influencing the biogeochemical conditions favoring DOP use as an organic nutrient. Specifically, surface ocean marine DOM exhibits increasingly P-depleted stoichiometries from east to west in the Pacific and from south to north in the Atlantic consistent with patterns of increasing P stress and alleviated iron stress, respectively.

1. Introduction

The ocean plays a critical role in the global carbon cycle, holding about fifty times as much carbon as does the atmosphere, and sequesters atmospheric carbon through its solubility and biological pumps (Hain et al., 2014; DeVries, 2022). The marine biological pump starts in the euphotic zone whereby phytoplankton transform inorganic carbon into organic matter through photosynthesis ("marine primary production"), followed by vertical export of that organic matter to the deep ocean ("marine export production") (Emerson, 2014; Hain et al., 2014; DeVries, 2022). Decades of effort have sought to understand the patterns and estimate the rates of marine primary production and

57 export production (e.g., Behrenfeld & Falkowski, 1997; Westberry et al., 2008; Emerson, 2014;

58 DeVries & Weber, 2017). However, considerable uncertainty in and discrepancy between

59 estimates of marine primary productivity and export productivity still exist (Carr et al., 2006;

60 Emerson, 2014; Siegel et al., 2023). In particular, the fields of biological and chemical

61 oceanography are still working to describe the processes that support marine primary and export

62 production in subtropical gyres where inorganic nutrients are scarce (Emerson, 2014).

63

64 A range of nutrient sources have been evaluated for their potential to support marine productivity

65 in subtropical gyres where nitrate (NO_3^-) and phosphate (PO_4^{3-}) concentrations are often at or

66 below detection limits, yet rates of export production are comparable to more nutrient-replete

67 regions (Gruber et al., 1998; Keeling et al., 2004; Johnson et al., 2010; Emerson, 2014). Candidate

68 sources include subsurface inorganic nutrients entrained by a range of physical mechanisms

69 (Kadko & Johns, 2011; Stanley et al., 2015; Mahadevan, 2016) and/or by vertically migrating

70 phytoplankton (Villareal et al., 1993; Wirtz et al., 2022), atmospheric deposition (Baker et al.,

71 2003; Knapp et al., 2010; Jickells & Moore, 2015), biological di-nitrogen (N_2) fixation (Knapp et

72 al., 2016, 2018b, 2021), and organic nutrients (Torres-Valdés et al., 2009; Lomas et al., 2010;

73 Letscher et al., 2016; Knapp et al., 2018a). While all of these mechanisms are thought to contribute

74 to marine production under different conditions, here we focus on evaluating the role of organic

75 nutrients. Phytoplankton may utilize dissolved organic nitrogen (DON) or dissolved organic

76 phosphorus (DOP) either after heterotrophic degradation that releases inorganic nutrients that are

77 then assimilated, or by the direct assimilation of DON and/or DOP. A wide range of marine

78 phytoplankton species including cyanobacteria, coccolithophores, diatoms, and dinoflagellates

79 utilize DON and DOP directly when the supply of inorganic nutrients is not sufficient to meet their

80 demands (e.g., Dyhrman et al., 2006; Bronk et al., 2007; Berges & Mulholland, 2008; Orchard et

81 al., 2010; Kathuria & Martiny, 2011; Li et al., 2018; Zhang et al., 2020b; Duhamel et al., 2021).

82 For example, phytoplankton have been shown to release extracellular alkaline phosphatase and C-

83 P lyase metalloenzymes to exploit P in DOP molecules (Dyhrman et al., 2006; Duhamel et al.,

84 2021), while for DON, phytoplankton may use leucine aminopeptidase to access N in peptides

85 (Bronk et al., 2007; Berges & Mulholland, 2008; Zhang et al., 2020b). While the significance of

86 organic nutrients in supporting marine production is expected to vary spatially, modeling studies

87 suggest that DOP uptake by phytoplankton sustains >50% of annual net community production in

88   the North Pacific and North Atlantic subtropical gyres (Torres-Valdés et al., 2009; Reynolds et al.,

89   2014; Letscher et al., 2016, 2022).

90

91   The preferential consumption of DON and DOP as nutrient sources stands in contrast to the

92   pressures on surface ocean dissolved organic carbon (DOC), which is primarily consumed by

93   heterotrophs. Consequently, the additional pressure on the DON and DOP pool by autotrophs is

94   expected to drive surface ocean DOM stoichiometry away from that of its source, autotrophic

95   production, and its associated "Redfield Ratio" stoichiometry (C:N:P = 106:16:1) (Redfield,

96   1934). Thus, interpreting variability in surface ocean dissolved organic matter (DOM)

97   stoichiometry may provide insight into conditions where utilization of DON and/or DOP supports

98   marine primary productivity. For instance, the bulk surface ocean DOC:DON:DOP ratio at Station

99   ALOHA in the North Pacific Ocean is ~350:24:1 (Foreman et al., 2019) and at the BATS station

100 in the North Atlantic Ocean is ~983:68:1 (Singh et al., 2015), both relatively depleted in N and P

101 compared with "Redfield" stoichiometry. Numerous additional observations and inversions

102 describing the variability in surface ocean organic matter stoichiometry have emerged in recent

103 years, often attributing the patterns to the plasticity of phytoplankton experiencing nutrient stress

104 (Martiny et al., 2013; Teng et al., 2014; DeVries & Deutsch, 2014; Galbraith & Martiny, 2015;

105 Inomura et al., 2022). However, most of these studies have investigated either marine particulate

106 or total organic matter. The examination of the patterns and causes of marine DOM stoichiometric

107 variability has been limited by the lack of global DON and DOP datasets, even though DOM is an

108 important component of the biological pump, accounting for ~20-25% of export productivity

109 (Carlson et al., 1994; Hopkinson & Vallino, 2005; Hansell et al., 2009; Letscher et al., 2015;

110 Roshan & DeVries, 2017; Siegel et al., 2023).

111

112 Here, we take advantage of new global surface ocean DOM datasets (Hansell et al., 2021; Liang

113 et al., 2022b) which permit evaluation of basin-scale trends in DOC, DON, and DOP distributions

114 and associated stoichiometry. The goals of this article are to: 1) describe basin-scale trends in

115 surface ocean DOM concentration and its C:N:P stoichiometry, and 2) evaluate mechanisms

116 consistent with inter-basin surface ocean DOM stoichiometric variability.

117

2. Methods

2.1 DOC, DON and DOP concentration datasets

The DOC and DON concentration data are from a recent compilation of global ocean observations from 1994 to 2021 (Hansell et al., 2021, version 1). The DOP concentration data are from the DOPv2021 database, which contains DOP concentration observations from 1990 to 2020 (Liang et al., 2022b). Only DOC concentration data marked with the "good" quality flag (WOCE bottle flag = 2) were used, and similar data screening processes were used for the DON and DOP concentration data. The remaining DOC, DON and DOP concentration data were binned onto the OCIM2 model grid with 2ºx2º horizontal resolution and 24 vertical layers (DeVries & Holzer, 2019; John et al., 2020) for further analysis. After gridding, there were 24,458 DOC concentration, 5,679 DON concentration, and 1,878 DOP concentration observations. Most DOM concentration observations are from the upper ocean with 40% of DOC, 87% of DON, and 87% of DOP observations from the upper 400 m.

2.2 Global ocean partitioning

To study variability in DOM stoichiometry across the surface ocean, we divided the global ocean into 10 biogeochemical or geographical regions. First we partitioned the global ocean into 10 biogeochemical regions according to Teng et al., 2014 and Letscher et al., 2022. The boundaries between regions correspond to the 0.3 µM surface ocean PO_4^{3-} concentration contour. The regions include the Atlantic Subarctic (AtlSub), the North Atlantic Subtropical Gyre (NASG), the Atlantic equatorial region (EqAtl), the South Atlantic Subtropical Gyre (SASG), the Pacific Subarctic (PacSub), the North Pacific Subtropical Gyre (NPSG), the Pacific equatorial region (EqPac), the South Pacific Subtropical Gyre (SPSG), the Indian Ocean (IND), and the Southern Ocean (SO). We also evaluated variability in DOM stoichiometry using geographical divisions, including the Eastern North Atlantic (ENATL, 0˚ - 65˚ N and 45˚ W – 10˚ E), the Eastern South Atlantic (ESATL, 0˚ - 40˚ S and 20˚ W – 20˚ E), the Western North Atlantic (WNATL, 0˚ - 65˚ N and 45˚ W -100˚ W), the Western South Atlantic (WSATL, 0˚ - 40˚ S and 20˚ W – 60˚ W), the Eastern North Pacific (ENPAC, 0˚ - 65˚ N and 70˚ E - 160˚ E), the Eastern South Pacific (ESPAC, 0˚ - 40˚ S and 70˚ E - 160˚ E), the Western North Pacific (WNPAC, 0˚ - 65˚ N and 100˚ W - 160˚ E), the

147 Western South Pacific (WSPAC, 0˚ - 40˚ S and 100˚ W - 160˚ E), the Indian Ocean (Indian, 40˚

148 S - 25˚ N and 20˚ E - 145˚ E), and the Southern Ocean (Southern, >40˚ S).

149

150 **2.3 Calculation of bulk and labile surface ocean DOC:DON:DOP concentration ratios**

151 Bulk and labile surface (<73 m) ocean DOC:DON:DOP concentration ratios were calculated for

152 each biogeochemical and geographical region. The upper 73 m was chosen to reflect the surface

153 ocean because the upper 73 m corresponds to the upper two vertical layers in the OCIM2 grid,

154 which are often used to represent the euphotic zone (DeVries & Holzer, 2019; Wang et al., 2019;

155 John et al., 2020; Letscher et al., 2022). For bulk DOC:DON:DOP concentration ratios, we

156 calculated the mean surface ocean bulk DOC, DON, and DOP concentrations in each region and

157 then used those to calculate mean DOC:DON:DOP concentration ratios in each region. For labile

158 DOC:DON:DOP concentration ratios, we subtracted the mean deep ocean bulk DOC, DON, and

159 DOP concentrations for each region from the mean surface ocean bulk DOC, DON and DOP

160 concentrations to get the mean surface ocean labile DOC, DON and DOP concentrations, and from

161 those the mean surface ocean labile DOC:DON:DOP concentration ratios were calculated for each

162 region. We assumed that the deep ocean DON concentration was 1.8 µM, which was taken as the

163 mean DON concentration in the deep ocean (>1000 m) according to Letscher & Moore, 2015, and

164 0.05 µM was taken as the mean deep ocean DOP concentration, which is the average deep ocean

165 (>1000 m) DOP concentration reported in the DOPv2021 database (Liang et al., 2022b). It is

166 known that deep ocean DOC concentrations decrease slightly along the global ocean conveyor belt

167 with highest DOC concentrations in the deep North Atlantic and lowest DOC concentrations in

168 the deep North Pacific (Hansell & Carlson, 1998b). Thus, we used different deep ocean DOC

169 concentrations to calculate surface labile DOC concentrations in each region. Concentrations of

170 deep ocean DOC were estimated at 44.4 µM in the North Atlantic, 41.5 µM in the South Atlantic,

171 39.6 µM in the Pacific, 42.2 µM in the Indian Ocean, and 41.9 µM in the Southern Ocean (Lønborg

172 et al., 2018). We did not include the Arctic Ocean in this study due to limited DOP concentration

173 observations from that basin.

174

2.4 Relationships between bulk surface ocean DOC, DON and DOP concentrations and Net Primary Productivity

We performed correlation analyses between gridded surface ocean bulk DOC, DON and DOP concentrations and rates of net primary production (NPP) (mol C m^{-2} yr^{-1}) by applying a Type II regression model in MATLAB with the function 'gmregress' (Trujillo-Ortiz & Hernandez-Walls, 2021). In order to test the robustness of the correlations between surface ocean bulk DOC, DON, and DOP concentrations and rates of NPP, we used climatological NPP fields from two algorithms: the Carbon-based Productivity Model (CbPM) (Westberry et al., 2008) and the Vertically Generalized Productivity Model (VGPM) (Behrenfeld & Falkowski, 1997), both estimated from SeaWiFS chlorophyll *a* observations. We did not include samples from the Arctic Ocean in this correlation analysis because it is known that DOC concentrations in the Arctic are significantly influenced by river discharge, an external source of DOC to the ocean (Anderson & Amon, 2015) and because of limited DOP concentration observations from this basin.

3. Results

3.1 **Global patterns in bulk surface ocean DOC, DON, and DOP concentration distributions**

Concentrations of DOC in the surface ocean reflect the balance of their sources and sinks. The primary source of DOC in the ocean is marine photosynthesis (Carlson & Hansell, 2015) with secondary coastal inputs that are especially pronounced in the Arctic (Hansell et al., 2004; Benner et al., 2005; Anderson & Amon, 2015) and other areas of significant riverine (Raymond & Spencer, 2015; Medeiros et al., 2015; Gledhill et al., 2022) and/or submarine groundwater discharge (Connolly et al., 2020). Marine DOC is lost due to heterotrophic consumption (Hansell & Carlson, 1998b; Carlson & Hansell, 2015), which results in progressive decreases in DOC concentration with depth and along circulation pathways (Hansell & Carlson, 1998b). Additionally, DOC can be lost due to photolysis (Mopper et al., 2015) or hydrothermal circulation (Lang et al., 2006). Our calculations of mean surface ocean DOC concentrations for each region based on the recent compilation of global DOC concentration data (Hansell et al., 2021) reflect the impact of these inputs, with relatively high concentrations, ~68 µM, in tropical and subtropical surface waters (40° S – 40° N), and relatively low concentrations in Southern Ocean surface waters, ~50 µM (Tables 1 & 2), consistent with previous observations and model output (Hansell et al., 2009; Roshan &

205   DeVries, 2017). We also note that the standard deviations of mean surface ocean DOC
206   concentrations in the EqAtl are high (73.5±21.6 µM), potentially resulting from the seasonally
207   variable input of DOC from the Amazon River (Raymond & Spencer, 2015; Gledhill et al., 2022).
208

209   While marine DON and DOP have the same source as DOC, and they share the same sinks as
210   DOC listed above, they can also be consumed by autotrophs as assimilative sources of N and P.
211   Indeed, autotrophic consumption of DON and DOP in the surface ocean appears to be significant
212   in the subtropical gyres when inorganic forms of N and P are scarce (Mather et al., 2008; Letscher
213   et al., 2013, 2022). Regardless, variations in mean surface ocean DON concentration among
214   regions are modest, with concentrations typically between 4.2 and 5.3 µM (Tables 1 & 2), also
215   consistent with previous observations (Letscher et al., 2013; Knapp et al., 2011; Knapp et al., 2018;
216   Bif et al., 2022). Mean regional surface ocean DON concentrations in the EqAtl and EqPac were
217   5.3±1.1 µM and 4.5±0.8 µM, respectively. In the NPSG, mean surface ocean DON concentrations
218   were 4.4±0.4 µM and in the SPSG were 4.2±0.5 µM (Table 1). The lowest mean surface ocean
219   DON concentrations were found in the SO, 3.7±0.8 µM (Tables 1 and 2).
220

221   In contrast, mean bulk surface ocean DOP concentrations showed more variability than DOC or
222   DON, with higher mean concentrations associated with regions of elevated upwelling and new
223   production. For example, mean surface ocean DOP concentrations in the EqPac were 0.27±0.06
224   µM, and in the EqAtl were 0.20±0.07 µM, and were lower in subtropical gyres, 0.11±0.07 µM in
225   the NASG and 0.15±0.07 µM in the SASG (Table 1), consistent with previous observations
226   (Björkman & Karl, 2003; Mather et al., 2008; Lomas et al., 2010; Hashihama et al., 2020; Liang
227   et al., 2022b). We note that the calculation of mean surface ocean DOP concentrations in the
228   AtlSub and IND were based on small data sets (n = 11 for AtlSub and n = 18 for IND) due to
229   limited observations from these two regions (Table 1). Additionally, DOP concentration
230   measurements in the AtlSub from the DOPv2021 database were collected at sites adjacent to the
231   NASG (Liang et al., 2022a), leading to potential bias. Further sampling for the Atlantic subpolar
232   region and Indian Ocean is required.
233

234   **3.2 Variations in bulk surface ocean DOM stoichiometry in different biogeochemical regions**

Bulk surface (< 73 m) ocean DOC:DON:DOP concentration ratios varied among biogeochemical regions (Figures 1a, b, c) (Table 3). DOC:DON concentration ratios in the different regions fell into a relatively narrow range, increasing by ~25% from 13.0:1 to 16.1:1, higher than the canonical Redfield ratio (C:N = 6.6:1), with relatively high DOC:DON concentration ratios found in the subtropical gyres, similar to previously reported bulk DOC:DON concentration ratios (Bif et al., 2022; Hansell & Carlson, 2001; Hopkinson & Vallino, 2005; Letscher & Moore, 2015). Bulk surface ocean DOC:DON concentration ratios in the NPSG, SPSG, NASG and SASG fell within a narrower range and were 15.5:1, 16.1:1, 14.6:1 and 15.3:1, respectively (Figure 1a) (Table 3). Bulk DOC:DON concentration ratios in equatorial and subpolar regions were slightly lower, 15.0:1 in the EqPac, 13.7:1 in the PacSub, 13.9:1 in the EqAtl, 13.0:1 in the AtlSub, and 14.2:1 in the SO (Figure 1a) (Table 3).

In contrast, bulk surface ocean DON:DOP concentration ratios were more variable than bulk surface ocean DOC:DON concentration ratios, and increased by ~175% from 17:1 in the EqPac to 44:1 in the AtlSub (Figure 1b) (Table 3). Bulk surface ocean DON:DOP concentration ratios in the PacSub were 21:1, in the SPSG were 22:1, and in the NPSG were 23:1 (Figures 1b, c) (Table 3). The Atlantic Ocean generally had higher DON:DOP concentration ratios than the Pacific. For example, the bulk surface ocean DON:DOP concentration ratios in the EqAtl were 27:1, in the SASG were 29:1, in the NASG were 43:1, and were 44:1 in the AtlSub (Figure 1b) (Table 3). We note that the high bulk surface ocean DON:DOP concentration ratios in the AtlSub were potentially biased by the limited DOP concentration observations in the region (n = 11, Table 1), with most of the observations collected near the neighboring subtropical gyre (NASG) (Liang et al., 2022b), which has elevated bulk surface ocean DOC:DOP and DON:DOP concentration ratios. Finally, bulk surface ocean DON:DOP concentration ratios were 19:1 in the IND and 21:1 in the SO (Figure 1b) (Table 3), intermediate between the EqPac and EqAtl values, and we also note that the majority of the IND samples were collected near the SO (Liang et al., 2022b).

As was seen for bulk surface ocean DON:DOP concentration ratios, bulk surface ocean DOC:DOP concentration ratios were also more variable than DOC:DON concentration ratios, and exhibited a 150% range from a low of 251:1 in the EqPac to a high of 638:1 in the NASG. Bulk surface ocean DOC:DOP concentration ratios in the PacSub were 293:1, and were higher in the NPSG and

266 SPSG, 358:1 and 356:1, respectively (Figure 1c) (Table 3). As was seen for DON:DOP, bulk
267 surface ocean DOC:DOP concentration ratios in the Atlantic were higher than in the Pacific. In
268 the EqAtl the bulk DOC:DOP concentration ratios were 368:1, in the SASG were 450:1, in the
269 AtlSub were 573:1, and in the NASG were 638:1 (Figure 1c) (Table 3). Finally, bulk surface ocean
270 DOC:DOP concentration ratios were 281:1 and 291:1 in the IND and SO, respectively (Figure 1c)
271 (Table 3).

272

273 In summary, bulk surface ocean DOM concentration ratios were depleted in N and P compared
274 with the canonical Redfield ratio (C:N:P = 106:16:1), and ranged from 251:17:1 in the EqPac to
275 638:43:1 in NASG (Table 3), with a global mean of 387:26:1 . Smaller regional variations in bulk
276 DOC:DON concentration ratios were observed than in bulk DON:DOP and DOC:DOP
277 concentration ratios, which were largely driven by changes in DOP concentration. Two patterns in
278 bulk surface ocean DOM stoichiometry emerged: 1) bulk DON:DOP and DOC:DOP concentration
279 ratios were lower in the equatorial and subpolar regions than those in the subtropical gyres; and,
280 2) bulk surface ocean DON:DOP and DOC:DOP concentration ratios were higher in the Atlantic
281 than in the Pacific (Figures 1b, c) (Table 3).

282

283 **3.3 Variations in bulk surface ocean DOM stoichiometry in different geographical regions**

284 Variations in bulk surface ocean DOM stoichiometry were also evaluated among geographical
285 divisions of ocean basins, which allowed us to compare stoichiometric differences between the
286 Western and Eastern or Southern and Northern regions of the Atlantic and Pacific Oceans, which
287 are not apparent from the biogeochemical divisions (Figures 1d, e, f). In the Atlantic Ocean, bulk
288 surface ocean DOC:DON concentration ratios showed no notable differences between Western
289 and Eastern regions or Southern and Northern regions, which were 15.7:1 in the WNATL, 13.1:1
290 in the ENATL, 15.2:1 in the WSATL, and 14.3:1 in ESATL (Table 4). A similarly narrow range
291 in bulk surface ocean DOC:DON concentration ratios was found in the Pacific Ocean, which
292 ranged from 14.5:1 to 16.1:1 (Table 4). Bulk surface ocean DOC:DON concentration ratios in the
293 WNPAC, ENPAC, WSPAC, and ESPAC were 15.3:1, 14.5:1, 16.1:1, and 15.4:1, respectively
294 (Figures 1-3).

295

296 Differences in bulk surface ocean DON:DOP concentration ratios in the Pacific were more

297 pronounced between the East and West than the North and South. In the ENPAC and ESPAC,

298 bulk surface ocean DON:DOP concentration ratios were 19:1 and 20:1, but increased to 25:1 and

299 27:1 in the WNPAC and WSPAC, respectively (Figure 1e) (Table 4). In contrast, differences

300 between bulk surface ocean DON:DOP concentration ratios were larger between the North and

301 South Atlantic regions compared to the Eastern and Western regions (Figure 1e) (Table 4). Bulk

302 surface ocean DON:DOP concentration ratios in the ESATL were 29:1 and in the WSATL were

303 31:1 while in the ENATL they were 39:1 and in the WNATL were 48:1 (Figure 1e) (Table 4).

304

305 Similar to DON:DOP, bulk surface ocean DOC:DOP concentration ratios had greater differences

306 between the Western and Eastern than between the Northern and Southern regions of the Pacific.

307 The bulk surface ocean DOC:DOP concentration ratios were 273:1 and 301:1 in the ENPAC and

308 ESPAC, respectively, while in the WNPAC they were 388:1 and in the WSPAC were 433:1

309 (Figure 1f) (Table 4). In contrast, differences in bulk surface ocean DOC:DOP concentration ratios

310 were larger between the North and South than between the East and West in the Atlantic Ocean

311 (Figure 1f) (Table 4). Bulk surface ocean DOC:DOP concentration ratios in the ESATL were 413:1

312 and in the WSATL were 467:1 while in the ENATL they were 515:1 and in the WNATL they

313 were 755:1 (Figure 1f) (Table 4). The relatively high bulk DOC:DOP and DON:DOP

314 concentration ratios found in the WNATL are consistent with the very low DOP concentrations

315 previously observed in Sargasso Sea (Mather et al., 2008; Lomas et al., 2010).

316

317 To further identify potential large-scale gradients in bulk surface ocean DOM stoichiometry, we

318 calculated zonal-mean, bulk surface ocean DOC:DON, DON:DOP, and DOC:DOP concentration

319 ratios in the Pacific, and meridional-mean, bulk surface ocean DOC:DON, DON:DOP, and

320 DOC:DOP concentration ratios in the Atlantic Oceans (Figures 2 and 3). In both cases, we used a

321 robust, locally weighted regression (LOWESS) in R (Cleveland, 1979) to fit the points along the

322 line of latitude or longitude to capture the zonal or meridional trends. Mean bulk surface ocean

323 DOC:DON concentration ratios in the Pacific exhibited limited variability (~50%), ranging from

324 ~12:1 to 18:1, but mean bulk surface ocean DON:DOP and DOC:DOP concentration ratios

increased ~100% when comparing ratios West vs. East of 160˚ W (Figure 2). In particular, mean bulk surface ocean DON:DOP concentration ratios increased from ~20:1 to ~40:1 from east to west of 160˚ W and mean bulk surface ocean DOC:DOP concentration ratios increased from ~250:1 to ~500:1 from east to west of 160 ˚W (Figure 2). In the Atlantic Ocean, the most pronounced DOM stoichiometric gradient occurred meridionally. While bulk surface ocean DOC:DON concentration ratios in the Atlantic Ocean were relatively invariant around ~15:1, bulk surface ocean DON:DOP and DOC:DOP concentration ratios increased ~100% from South to North, reaching maxima of ~45:1 and ~700:1, respectively, between 20˚ N and 40˚ N compared to ratios observed between 30˚ S to 20˚ S, ~25:1 and 350:1, respectively (Figure 3). The majority of these increases in DON:DOP and DOC:DOP concentration ratios were driven by decreasing DOP concentrations between the South and North Atlantic.

In summary, two patterns were identified from the geographical divisions that were not clear from the biogeochemical divisions: 1) bulk surface ocean DOC:DON:DOP concentration ratios increased from ~250:20:1 in the East to ~500:40:1 in the West in the Pacific Ocean, and, 2) bulk surface ocean bulk DOC:DON:DOP concentration ratios increased meridionally from South to North in the Atlantic Ocean to maxima of ~700:45:1 between 20˚ N and 40˚ N.

3.4 Relationships between surface ocean DOM concentrations and rates of NPP

To evaluate patterns in DOM production and consumption, we calculated correlations of bulk surface ocean DOC, DON, and DOP concentrations vs. satellite-derived rates of NPP using the Carbon-based Productivity Model (CbPM) (Westberry et al., 2008). Given that NPP is the primary source of DOM to the surface ocean (Carlson & Hansell, 2015), it is not surprising that bulk surface ocean DOC, DON, and DOP concentrations are all statistically significantly correlated with rates of NPP (Figure 4). Indeed, similar results have been previously observed for DOC (Hansell & Carlson, 1998a), DON (Knapp et al., 2018a; Zhang et al., 2020a), and DOP (Liang et al., 2022a). However, since DON and DOP are also quantitatively important assimilative nutrient sources for autotrophs, their correlations are not as strong as between DOC and NPP rate estimates; the correlations between bulk surface ocean DOC, DON, and DOP concentrations and CbPM-derived

354   rates of NPP had $R^2 = 0.41$, p <0.0000001, $R^2 = 0.28$, p <0.0000001, and $R^2 = 0.09$, p <0.0000001,

355   respectively, evaluated using Type II regression model (reduced major axis regressions) (Figure

356   4). Importantly, the y-intercepts for the relationships between bulk surface ocean DOC and DON

357   concentrations and CbPM-derived NPP rates were 46 uM and 2.8 uM, respectively, consistent

358   with the concentration of deep ocean (>1000 m), "refractory" DOC and DON calculated from the

359   DOC and DON concentrations database (Hansell et al., 2021) (Table 5). However, the y-intercept

360   for the relationship between bulk surface ocean DOP concentration and CbPM-derived NPP rates

361   was a small negative number (-0.05 μM), which is nonsensical. We note that a number of surface

362   ocean DOP concentration data from the North Atlantic fall below the best fit regression line while

363   data from the Eastern Pacific fall above the line, contributing to the negative intercept (Figure 4c).

364   Low DOP concentrations were observed in the North Atlantic, consistent with previous

365   observations of elevated rates of DOP consumption due to elevated PO_4^{3-} stress (Dyhrman et al.,

366   2006; Van Mooy et al., 2009; Lomas et al., 2010; Sohm & Capone, 2010; Liang et al., 2022a),

367   which contributes to the negative y-intercept. To address this issue but still capture the relationship

368   between estimated rates of NPP and bulk surface ocean DOP concentrations, we set the intercept

369   to 0.05 μM, which corresponds to the deep ocean (>1000 m) DOP concentration observed at

370   Station ALOHA (Foreman et al., 2019) as well as that calculated from the DOPv2021 database

371   (Liang et al., 2022b), and then refitted the linear regression.

372

373   After forcing the y-intercept of the regression between surface ocean DOP concentration and

374   CbPM estimated rates of NPP through 0.05 μM, the ratios of the three slopes in Figures 4a, b and

375   c are C:N:P = 173:15.5:1, and the ratio of the y-intercepts is 920:56:1. Here, we consider the

376   stoichiometry of the y-intercepts to reflect the DOC:DON:DOP concentration ratios of

377   "refractory", or deep-ocean DOM, where rates of NPP = 0. In contrast, the ratio of the slopes can

378   be considered the DOC:DON:DOP concentration ratio of "labile" surface ocean DOM, or the

379   stoichiometry of the incrementally added DOM that results from increasing rates of NPP. Using

380   the VGPM NPP product (Behrenfeld & Falkowski, 1997) did not meaningfully alter the strength

381   of the correlation between DOC, DON, and DOP concentrations vs. rates of NPP ($R^2 = 0.36$, p <

382   0.0000001 for DOC vs. NPP, $R^2 = 0.28$, p < 0.0000001 for DON vs. NPP, and $R^2 = 0.07$, p <

383 0.0000001 for DOP vs. NPP), or the labile or refractory DOM C:N:P ratios calculated from this

384 method (Table 5). Our labile DOC:DON:DOP concentration ratios calculated by this approach are

385 also similar to those reported in Hopkinson & Vallino, 2005, 199:20:1. However, our refractory

386 DOC:DON:DOP concentration ratios are much lower than those that reported in Hopkinson &

387 Vallino, 2005, 3511:202:1, probably in part due to the majority of their samples being collected

388 in the North Atlantic, where the highest global ocean bulk DON:DOP and DOC:DOP

389 concentration ratios and lowest DOP concentrations are found (Figure 1). However, our refractory

390 DOC:DON:DOP concentration ratios calculated by this approach are consistent with the carefully

391 measured deep ocean DOC:DON:DOP concentration ratios via improved methods at Station

392 ALOHA, C:N:P = 760:45:1 (Foreman et al., 2019) .

393

394 **3.5 Variations in labile surface ocean DOM stoichiometry in different biogeochemical**

395 **regions**

396 Correlations between surface ocean DOC, DON, and DOP concentrations and rates of NPP

397 indicate that DOC, DON and DOP can be divided into labile and refractory pools, and here we

398 specifically explore the stoichiometry of labile surface ocean DOM. Removing the "inertia" of the

399 recalcitrant DOM from surface ocean stoichiometry allows us to focus on variability associated

400 with DOC:DON:DOP production and consumption patterns unique to biogeochemically and

401 geographically defined regions. Here we estimate labile surface ocean DOC, DON, and DOP

402 concentrations by subtracting the mean deep ocean concentrations from the mean surface ocean

403 concentrations, as has been done previously (Lønborg et al., 2018; Letscher et al., 2022). We find

404 that regional variations in labile surface ocean DOM stoichiometry are similar to those observed

405 for bulk surface ocean DOM stoichiometry, with generally lower ratios found in the equatorial and

406 subpolar regions and higher concentration ratios found in the subtropical gyres (Figures 5a, b, c)

407 (Table 6). Additionally, labile surface ocean DOM had higher DON:DOP and DOC:DOP

408 concentration ratios but lower DOC:DON concentration ratios in the Atlantic Ocean than in the

409 Pacific Ocean (Figures 5a, b, c) (Table 6).

410

411 Broadly speaking, labile surface ocean DOC:DON concentration ratios were lower, and thus closer

to the "Redfield" C:N ratio of 6.6:1 than the bulk DOC:DON concentration ratios, and ranged from 5.4:1 to 12.0:1, or spanned a ~100% range, a larger dynamic range than was observed for bulk surface ocean DOC:DON concentration ratios. Specifically, in the IND and SO, labile surface ocean DOC:DON concentration ratios were 9.2:1 and 5.4:1, respectively (Figure 5a) (Table 6). In the EqPac and EqAtl, labile surface ocean DOC:DON concentration ratios were 10.6:1 and 8.4:1, respectively, and in the PacSub and AtlSub were 8.1:1 and 7.0:1, respectively (Figure 5a) (Table 6). In the NPSG and SPSG, labile surface ocean DOC:DON concentration ratios were 11.0:1 and 12.0:1, respectively, and in the NASG and SASG they were 8.5:1 and 9.8:1, respectively (Figure 5a) (Table 6).

As was seen for labile surface ocean DOC:DON concentration ratios, labile surface ocean DON:DOP concentration ratios were also lower than was seen in the bulk pool, ranged from 12:1 to 50:1, and thus were closer to the "Redfield" N:P ratio of 16:1. Generally, labile surface ocean DON:DOP concentration ratios were lowest near regions of significant upwelling and/or new production, and were higher in the subtropical gyres. For example, in the EqPac and EqAtl, labile surface ocean DON:DOP concentration ratios were 12:1 and 23:1, respectively, and in the IND and SO were both 15:1 (Figure 5b) (Table 6). In the PacSub and AtlSub, labile surface ocean DON:DOP concentration ratios diverged between the basins, and were 17:1 and 50:1, respectively. However, this Atlantic/Pacific difference needs further investigation due to limited DOP observations in the AtlSub (n=11, Table 1). This Atlantic/Pacific difference is also observed in the subtropical gyres, with NPSG and SPSG labile surface ocean DON:DOP concentration ratios of 19:1 and 17:1, respectively, while in the SASG and NASG they were 26:1 and 49:1, respectively. We note that labile surface ocean DON:DOP concentration ratios in the EqPac are lower than the canonical Redfield ratio, 12:1, which has not been reported before and is lower than the reported PON:POP ratios of ~22:1 in the Pacific equatorial region (Lee et al., 2021).

Similar to DOC:DON and DON:DOP, mean labile surface ocean DOC:DOP concentration ratios observed in the biogeochemical regions were lower than the bulk surface ocean DOC:DOP concentration ratios, and ranged from 83:1 to 414:1 (Table 6), and thus were closer (and sometimes

even lower than) the "Redfield" C:P ratio of 106:1. As was seen previously, lower mean labile surface ocean DOC:DOP concentration ratios were observed in regions associated with upwelling and higher rates of NPP, and increased in the subtropical gyres. Specifically, in the EqPac and EqAtl, the mean labile surface ocean DOC:DOP concentration ratios were relatively low, 127:1 and 195:1, respectively, similar to those in the IND and SO, 138:1 and 83:1, respectively (Figures 5c) (Table 6). Labile surface ocean DOC:DOP concentration ratios increased in the subpolar gyres, 139:1 in the PacSub and 346:1 in the AtlSub (Figure 5c) (Table 6). In the NPSG and SPSG, labile surface ocean DOC:DOP concentration ratios were both 209:1 and in the NASG and SASG they were 414:1 and 254:1, respectively (Figure 5c) (Table 6). In the SO, labile surface ocean DOC:DOP and concentration ratios (C:P = 83:1) were also lower than the canonical Redfield ratio. However, lower-than Redfield POM C:P ratios have also been reported from the Southern Ocean in previous work (POM C:P = 91:1 in Teng et al., 2014, and POM C:P = 61:1 - 190:1 in Lee et al., 2021).

In summary, labile surface ocean DOC:DON:DOP concentration ratios ranged from 83:15:1 to 414:49:1 among biogeochemically divided regions, with a global mean of 179:20:1, and with typically lower stoichiometric ratios than in the bulk pool, with the low DOP concentrations observed in the NASG and AtlSub driving maxima in labile DON:DOP and DOC:DOP concentration ratios (Figure 5) (Table 6).

3.6 Variations in surface ocean labile DOM stoichiometry in different geographical regions

Regional variations in labile surface ocean DOM stoichiometry in the geographical regions are similar to those observed in the biogeochemical regions, with concentration ratios closer to the canonical Redfield ratio than the bulk DOM concentration ratios observed in the same regions (Figures 5d, e, f) (Table 7). As was apparent in the bulk surface ocean DOM stoichiometry, the geographical divisions again highlight labile DOM stoichiometric gradients between the Eastern and Western Pacific, and between the Southern and Northern Atlantic Oceans.

470   Surface ocean labile DOC:DON concentration ratios in the geographical regions ranged from 4.8
471   to 12.1, and were generally lower near regions of elevated rates of NPP, most notably in the
472   Southern region where labile surface ocean DOC:DON concentration ratios were 4.8:1 (Table 7).
473   In the Pacific Ocean, we found no notable differences in labile surface ocean DOC:DON
474   concentration ratios between the Northern and Southern or Eastern and Western geographic
475   regions. Surface ocean labile DOC:DON concentration ratios in the ENPAC and ESPAC were
476   9.6:1 and 10.9:1, respectively, and in the WNPAC and WSPAC were 10.6:1 and 12.1:1,
477   respectively (Table 7). In the Atlantic Ocean, differences in labile surface ocean DOC:DON
478   concentration ratios are also small. In the ENATL and ESATL, labile surface ocean DOC:DON
479   concentration ratios were 7.1:1 and 8.9:1, respectively and in the WNATL and WSATL labile
480   surface ocean DOC:DON concentration ratios were 10.5:1 and 10.1:1, respectively.

481

482   Similar to bulk surface ocean DON:DOP concentration ratios, labile surface ocean DON:DOP
483   concentration ratios, which ranged from 14:1 to 58:1, were more variable than labile surface ocean
484   DOC:DON concentration ratios. However, labile surface ocean DON:DOP concentration ratios
485   were not meaningfully lower than bulk surface ocean DON:DOP ratios. Relatively low labile
486   surface ocean DON:DOP concentration ratios were observed in the Indian and SO, 14.8 and 19.3,
487   respectively (Figure 5) (Table 7). In the Pacific Ocean, there were larger differences between labile
488   surface ocean DON:DOP concentration ratios in the East vs. West than between the North vs.
489   South, similar to the bulk pool (Figure 5). Labile surface ocean DON:DOP concentration ratios in
490   the ENPAC and ESPAC were both 14:1 but increased to 22:1 in the WNPAC and WSPAC (Figure
491   5) (Table 7). In the Atlantic the difference in labile surface ocean DON:DOP concentration ratios
492   was most pronounced between the North vs. South. The ESATL and WSATL had labile surface
493   ocean DON:DOP concentration ratios of 26:1 and 27:1, while the ENATL and WNATL had labile
494   surface ocean DON:DOP concentration ratios of 42:1 and 58:1, respectively (Figure 5) (Table 7).

495

496   Similar patterns were observed for labile surface ocean DOC:DOP concentration ratios, which
497   ranged from 93:1 to 610:1, and were generally higher in the Western vs. Eastern Pacific, and
498   Northern vs. Southern Atlantic. Again, the lowest labile surface ocean DOC:DOP concentration
499   ratios were found in the Southern and IND regions, 93:1 and 135:1, respectively. In the Pacific

500 Ocean, labile surface ocean DOC:DOP concentration ratios in the ENAPC and ESPAC were 134:1

501 and 154:1, respectively, and increased to 228:1 and 270:1 in the WNPAC and WSPAC,

502 respectively (Figure 5) (Table 7). In the Atlantic Ocean, the labile surface ocean DOC:DOP

503 concentration ratios in the ESATL and WSATL were 228:1 and 276:1, while in the ENATL and

504 WNATL they were 299:1 and 610:1, respectively (Figure 5) (Table 7).

505

506 In summary, the labile surface ocean DOC:DON:DOP concentration ratios in the geographically

507 defined regions ranged from 93:19:1 in the Southern Ocean to 610:58:1 in the WNATL (Table 7),

508 and were typically closer to "Redfield" stoichiometry than the bulk surface ocean DOC:DON:DOP

509 concentration ratios (268:19:1 to 745:47:1) (Table 4). Labile surface ocean DON:DOP and

510 DOC:DOP stoichiometry shared similar patterns to their bulk counterparts, and increased from

511 East to West in the Pacific Ocean and from South to North in the Atlantic Ocean, with the highest

512 labile surface ocean DON:DOP and DOC:DOP stoichiometry found in the Sargasso Sea (20º N –

513 40º N) of the WNATL.

514

515 **4. Discussion**

516 **4.1 Variability in bulk surface ocean DOM stoichiometry driven by changes in surface**

517   **ocean DOP concentrations**

518 Previous work has examined variability in bulk surface ocean DOC and DON concentrations as

519 well as their concentration ratios, finding relatively small variations in DON concentrations and

520 DOC:DON concentration ratios (Hansell & Carlson, 2001; Letscher et al., 2013; Sipler & Bronk,

521 2015; Bif et al., 2022). We similarly find relatively low variability in both bulk and labile surface

522 ocean DOC:DON concentration ratios (Figures 1 & 4) (Tables 1-6). Evaluating bulk global surface

523 ocean DOC and DON concentration data together with new DOP concentration data (Liang et al.,

524 2022b), we find that bulk and labile surface ocean DON:DOP and DOC:DOP concentration ratios

525 vary more than bulk and labile surface ocean DOC:DON concentration ratios, indicating that

526 variations in DON:DOP and DOC:DOP concentration ratios are driven by the relatively wide

527 range in DOP concentrations compared to the ranges in surface ocean DOC and especially DON

528 concentrations (Figures 1 and 4) (Tables 3-7). Indeed, according to the global ocean DOC, DON

529 and DOP concentration datasets (Hansell et al., 2021; Liang et al., 2022b), the typical range in

530 bulk surface ocean DOC, DON and DOP concentrations are 40 – 80 µM, 3 – 6 µM and 0.05 – 0.6

531 µM, respectively. These concentration ranges correspond to a 100% increase between typical

532 surface ocean DOC and DON minimum and maximum concentrations, but a 1100% increase

533 between the typical minimum and maximum surface ocean DOP concentrations. Thus, the order

534 of magnitude larger variability in bulk surface ocean DOP concentrations relative to bulk surface

535 ocean DOC and DON concentrations corresponds to the higher variability in surface ocean

536 DON:DOP and DOC:DOP concentration ratios relative to bulk surface ocean DOC:DON

537 concentration ratios.

538

539 We hypothesize that high variability in bulk surface ocean DON:DOP and DOC:DOP

540 concentration ratios is driven by the changes in DOP concentrations due to DOP consumption by

541 phytoplankton in the surface ocean. To evaluate this, we compared bulk surface ocean DON:DOP

542 and DOC:DOP concentration ratios with a model product of the estimated fraction of annual net

543 community production (ANCP) supported by DOP consumption (Letscher et al., 2022) in different

544 biogeochemical regions (Figure 6). Although no correlation for the global data set was found, we

545 found positive correlations between bulk surface ocean DOC:DOP concentration ratios and the

546 model-estimated fraction of ANCP supported by DOP consumption for points in the Pacific Ocean

547 (R^2=0.89, slope = 1347, p<0.05) as well as separately for the Atlantic Ocean (R^2=0.85, slope =

548 1987, p <0.05) (Figure 6). Similarly, positive correlations between DON:DOP concentration ratios

549 and the model estimated fraction of ANCP supported by DOP consumption were also found for

550 points in the Pacific Ocean (R^2=0.88, slope = 68, p<0.05) and separately for the Atlantic Ocean

551 (R^2=0.67, slope = 147, p<0.05) (Figure 6). These positive correlations between bulk surface ocean

552 DOC:DOP or DON:DOP concentration ratios and the fraction of ANCP supported by DOP

553 consumption by surface ocean phytoplankton supports the conclusion that DOP consumption by

554 phytoplankton is the major contributor to changes in bulk surface ocean DOP concentrations, and

555 the associated changes in bulk surface ocean DOC:DOP and DON:DOP concentration ratios. We

556 interpret the higher bulk surface ocean DOC:DOP and DON:DOP concentration ratios and

557 associated y-intercepts in Figure 6 for the Atlantic Ocean relative to the Pacific to imply that the

558 Atlantic Ocean has a more P-depleted 'preformed' character relative to the Pacific Ocean,

19

559 consistent with elevated rates of dissimilatory N loss in the Pacific vs. Atlantic (see section 4.2

560 below). Quantitatively, the slopes above suggest that for a 10% increase in the fraction of ANCP

561 supported by DOP consumption in the Atlantic Ocean, DON:DOP and DOC:DOP concentration

562 ratios increase by 15:1 and 135:1, respectively. In the Pacific Ocean, DON:DOP and DOC:DOP

563 concentration ratios increase by 7:1 and 15:1, respectively, with a 10% increase in the fraction of

564 ANCP supported by the DOP consumption. We suggest that these relatively large changes in

565 surface ocean DOP concentrations due to autotrophic DOP consumption contribute to the zonal

566 and meridional mean trends in bulk and labile surface ocean DON:DOP and DOC:DOP

567 concentration ratios observed in the Pacific Ocean and Atlantic Ocean, respectively (Figures 3 and

568 4), which are explored further below.

569

570 **4.2 Linkage between bulk and labile surface ocean DOM stoichiometry and water column**

571   **denitrification in the Pacific Ocean**

572 As reported here, the Pacific Ocean experiences greater West to East variability in bulk and labile

573 surface ocean DOM stoichiometry than between the North and South (Figure 1) (Tables 3 and 4).

574 In particular, higher bulk surface ocean DOP concentrations are observed East vs. West of ~160°

575 W (Figure 2). These gradients in bulk surface ocean DOP concentration correspond to large

576 gradients in bulk and labile surface ocean DON:DOP and DOC:DOP stoichiometry zonally across

577 the Pacific Ocean, with lower ratios in the Eastern vs. Western Pacific Ocean (Figure 2). Previous

578 work has suggested that zonal changes in DOP concentration across the Pacific can be attributed

579 to the net production and accumulation of DOP in surface waters over oxygen deficient zones

580 (ODZs), driven by dissimilatory NO_3^- consumption in suboxic subsurface waters (Liang et al.,

581 2022a). The ODZs of both the Eastern Tropical North Pacific (ETNP) and Eastern Tropical South

582 Pacific (ETSP) support significant rates of water column denitrification and/or anaerobic

583 ammonium oxidation (Ward et al., 2009; Chang et al., 2010, 2012; DeVries et al., 2012) (Figure

584 2). The resulting supply of a relative excess of PO_4^{3-} compared to NO_3^- and "Redfieldian"

585 phytoplankton demands in waters upwelled to the surface puts low pressure on the DOP pool as

586 an assimilative source of P, and allows accumulated DOP to be advected west, where slow but

587 progressive DOP consumption gradually reduces bulk surface ocean DOP concentrations (Liang

588 et al., 2022a). At basin scales, this corresponds to zonal increases in bulk surface ocean DON:DOP

589 and DOC:DOP concentration ratios from East to West (Figure 2).

590

591 In addition to direct measurements and modeled estimates of rates of water column

592 denitrification and anammox, geochemical tracers such as "P*", where P* = ($[PO_4^{3-}]$ – $[NO_3^{-}$

593 $]$/16), record the effects of water column denitrification and/or anaerobic ammonium

594 oxidation (Deutsch et al., 2007). Here we compare modeled rates of water column

595 denitrification (Wang et al., 2019) and zonally averaged surface ocean P* values calculated

596 using World Ocean Atlas 2013 nutrient data (Garcia et al., 2013) with zonal trends in bulk

597 surface ocean DON:DOP and DOC:DOP concentration ratios (Figure 7). Results show that

598 Spearman's correlation coefficients for both zonal mean bulk surface ocean DON:DOP and

599 DOC:DOP concentration ratios vs. rates of water column denitrification are -0.58 ($p < 0.001$).

600 Similarly, Spearman's correlation coefficients for both zonal mean bulk surface ocean

601 DON:DOP and DOC:DOP concentration ratios vs. P* are -0.55 ($p < 0.001$), indicating

602 significant negative correlations between zonal trends of bulk surface ocean DON:DOP and

603 DOC:DOP concentration ratios and rates of water column denitrification and P* in the Pacific

604 Ocean (Figure 7). Similar results are found when comparing labile surface ocean DOM

605 stoichiometry with P* and modeled denitrification rates (Spearman's correlation coefficients

606 = -0.56, $p < 0.001$ for labile DON:DOP/DOC:DOP vs. rates of water column denitrification

607 and Spearman's correlation coefficients = -0.53, $p < 0.001$ for labile DON:DOP/DOC:DOP

608 vs. P*).

609

610 The linkage between the surface ocean DOM stoichiometry and water column denitrification

611 rates is also apparent when comparing patterns in DOM stoichiometry in the Pacific Ocean

612 with the Atlantic Ocean. The minimum oxygen concentration in the water column in the

613 Eastern Atlantic is not low enough to enable denitrification (Zehr & Ward, 2002; Paulmier &

614 Ruiz-Pino, 2009; DeVries et al., 2012), which results in a reduced supply of excess PO_4^{3-} to

615 surface waters relative to the supply of NO_3^{-} and Redfieldian phytoplankton demands.

616 Without significant rates of dissimilatory N loss in the water column of the Eastern Atlantic

617 reducing pressure on the surface ocean PO_4^{3-}, and thus DOP pools, we do not observe

618 significant zonal gradients in bulk and labile DON:DOP and DOC:DOP concentration ratios

619 between the Eastern and Western Atlantic (Figure 1). Instead, we observe relatively elevated

bulk surface ocean DON:DOP concentration ratios in the Eastern Atlantic (~30:1-40:1) relative to the Eastern Pacific, 19:1 (Table 4), with similar trends observed for bulk surface ocean DOC:DOP concentration ratios (Table 4). We interpret this to result from increased pressure on the DOP pool in the Eastern Atlantic due to higher PO_4^{3-} stress. Consequently, we argue that water column denitrification in the ETNP and ETSP leaves a signature in bulk and labile surface ocean DOM stoichiometry that effectively leads to a "subsidy" of DOP in Pacific surface waters that may support elevated rates of carbon and nitrogen fixation compared to the Atlantic.

Although low surface ocean PO_4^{3-} concentrations and thus elevated P stress are the primary drivers of DOP consumption, recent work suggests that alleviated iron stress can enhance surface ocean DOP consumption (Liang et al., 2022a). In Figure 7 we overlay the zonal trends of 12 modeled dust deposition rates (Xu & Weber, 2021), as well as satellite derived NPQ-corrected φ_{sat}, a remote-sensing based estimate of iron stress experienced by phytoplankton (Behrenfeld et al., 2009; Liang et al., 2022a), to explore their relationships with surface ocean DOP distributions. Since modeled dust deposition patterns and rates are highly dependent on model choice, we consider the dust deposition output from 12 different atmospheric models (Xu & Weber, 2021). These 12 atmospheric models include 10 models from the AEROCOM Phase II Intercomparison project and two estimates from Mahowald et al., 2005 and Zhang et al., 2015. NPQ-corrected φ_{sat} has been used to indicate iron stress experienced by marine phytoplankton (Behrenfeld et al., 2009; Browning et al., 2014; Hopwood et al., 2018; Lee et al., 2021; Liang et al., 2022a) based on phytoplankton photochemical and physiological relationships (Behrenfeld & Milligan, 2013), where higher NPQ-corrected φ_{sat} values correspond to elevated iron stress faced by phytoplankton. We find that dust deposition rates increase and NPQ-corrected φ_{sat} decreases from East to West across the Pacific Ocean (Figure 7). Gradients in both metrics suggest that phytoplankton experience less iron stress in the Western than Eastern Pacific Ocean, consistent with observations that iron limits phytoplankton growth (Mahowald et al., 2005; Moore et al., 2013; Ustick et al., 2021) and nitrogen fixation rates (Knapp et al., 2016) in the Eastern Pacific Ocean. We note that hydrothermal vents along the Tonga-Kermadec Ridge in the Western Pacific Ocean are another potential source of iron in addition to dust deposition (Guieu et al., 2018). Thus, we interpret the increasing bulk and labile surface ocean DON:DOP and DOC:DOP stoichiometry

651 from East to West in the Pacific Ocean to result from progressive DOP consumption, in particular

652 as PO_4^{3-} stress increases and iron stress decreases zonally.

653

654 **4.3 Linkage between bulk and labile DOM stoichiometry and iron supply in the Atlantic**

655 **Ocean**

656 Here we explore potential causes of the meridional as opposed to zonal gradients in bulk and

657 labile surface ocean DOM stoichiometry observed in the Atlantic Ocean. In the Atlantic

658 Ocean the maxima in bulk and labile surface ocean DON:DOP and DOC:DOP concentration

659 ratios were found in the Sargasso Sea (20˚ N- 40˚ N) (Figures 3 and 8), coincident with the

660 extraordinarily low DOP concentrations previously observed in this region, ~50 nM (Mather

661 et al., 2008; Lomas et al., 2010; Liang et al., 2022b) (Figure 3). Indeed, the Sargasso Sea is the

662 region where the highest bulk and labile surface ocean DON:DOP and DOC:DOP

663 stoichiometry is found not just in the Atlantic Ocean, but in the global ocean (Figures 1 and

664 2), highlighting the unique nature of this region . Previous work suggested that enhanced DOP

665 consumption in this region occurs when phytoplankton face increased PO_4^{3-} stress but iron

666 stress is alleviated (Liang et al., 2022a). Similar to our analysis in the Pacific Ocean, we use

667 meridionally-averaged, modeled dust deposition rates (Xu & Weber, 2021), NPQ-corrected

668 φ_{sat} (Behrenfeld et al., 2009; Liang et al., 2022a), and surface ocean P* calculated from World

669 Ocean Atlas 2013 (Garcia et al., 2013) to evaluate iron and PO_4^{3-} stress, respectively, in the

670 Atlantic Ocean.

671

672 The minima in Atlantic surface ocean P* is found between 20˚ N and 40˚ N (Figure 8), indicative

673 of elevated PO_4^{3-} stress in this region. The maxima of dust deposition rates estimated from the 12

674 models converged between 0˚ and 20˚ N, and NPQ-corrected φ_{sat} also decreases between 20˚ N

675 and 40˚ N (Figure 8), suggesting reduced iron stress in this region. The maxima of DOC and DON

676 concentrations in the Atlantic Ocean were also found between 0˚ N and 20˚ N, consistent with

677 regional dust fertilization of phytoplankton (Figures 3 & 8). However, no notable increase in DOP

678 concentrations are observed between 0˚ and 20˚ N, and the maxima in DON:DOP and DOC:DOP

679 concentration ratios are found between 20˚ N and 40˚ N. We interpret these meridional trends to

680 indicate that reduced iron stress from dust deposition enhances primary productivity to the extent

681 that phytoplankton can access adequate N and P, from either inorganic or organic sources. Between

682   20° N to 40° N, consumption of DOP increases due to elevated PO_4^{3-} stress, with a resulting

683   surface ocean DOM stoichiometric signature of extraordinarily elevated bulk and labile DON:DOP

684   (up to ~58:1) and DOC:DOP (up to ~745:1) concentration ratios (Figure 8). We suggest that other

685   regions with relatively elevated bulk and labile surface ocean DON:DOP (~27-30:1) and

686   DOC:DOP (~400:1) concentration ratios, e.g., the Western North and South Pacific and Western

687   South Atlantic (Figures 1 and 5) (Tables 3,4, 6 & 7) would continue to draw down surface ocean

688   DOP concentrations if iron were more abundant.

689

690   **4.4 Comparison between surface ocean DOM and POM stoichiometry**

691   Finally, we compare our results in bulk and labile surface ocean DOM stoichiometry with POM

692   stoichiometry. Recent studies show that surface ocean POM C:N:P stoichiometry exhibits regional

693   variability depending on nutrient stress and phytoplankton community composition (Teng et al.,

694   2014; Galbraith & Martiny, 2015; Lomas et al., 2021; Inomura et al., 2022). Here, we use recent

695   global POM concentration datasets (Martiny et al., 2014; Tanioka et al., 2022) to calculate surface

696   ocean POC:PON:POP stoichiometry in the same 10 biogeochemical regions (Table S1) and

697   compare them with the bulk and labile surface ocean DOC:DON:DOP stoichiometry (Figure 9).

698   First, we find that bulk DOC:DON concentration ratios (C:N = 14.6:1) are higher than labile

699   DOC:DON and POC:PON concentration across all regions, with labile DOC:DON and POC:PON

700   concentration ratios more similar to each other, mean of 8.9:1 for labile DOC:DON and 7.7:1 for

701   POC:PON (Figure 9) (Table S1). These results suggest that labile DOM and POM are produced

702   with similar C:N ratios, with refractory DOM becoming more depleted in N either from

703   preferential remineralization (Letscher & Moore, 2015, Knapp et al., 2018), and/or potentially

704   accumulating DOC from another source (McCarthy et al., 2004). We also note that labile

705   DOC:DON concentration ratios are systematically higher than POC:PON concentration ratios in

706   the Pacific than Atlantic Ocean (Figure 9). We hypothesize that this results from preferential loss

707   of surface ocean DON resulting from increased pressure on the surface ocean DON pool due to

708   dissimilatory inorganic N loss in the ODZs of the Eastern Pacific (Knapp et al., 2018a; Bif et al.,

709   2022), although additional field work would help evaluate this possibility.

710

711   Additionally, we find that labile DOM, bulk DOM, and POM have similar N:P stoichiometry

712   across different biogeochemical regions, with the exception of the NASG, where labile and bulk

713   DON:DOP stoichiometry (N:P = 43:1 for bulk DOM and N:P=49:1 for labile DOM) exceed

714   PON:POP stoichiometry (N:P = 31:1) (Figure 9) (Table S1), suggesting that the NASG is a unique

715   region with significant DOP consumption by phytoplankton. Typically, bulk DOC:DOP

716   stoichiometry (global mean of 387:1) is higher than labile DOC:DOP and POC:POP stoichiometry

717   (global mean of 179:1 for labile DOC:DOP and global mean of 160:1 for POC:POP), which are

718   similar across the different biogeochemical regions (Figure 9). However, the NASG exhibits

719   higher labile DOC:DOP stoichiometry (C:P = 638:1) than POC:POP (C:P = 285:1), which we

720   hypothesize results from autotrophic DOP consumption. We argue that the reduced P* and

721   elevated dust deposition to the NASG sets it apart in the global ocean and places extreme pressure

722   on the surface ocean DOP pool as alternative autotrophic nutrient sources, consistent with previous

723   studies on DOP cycling in the Sargasso Sea (Mather et al., 2008; Van Mooy et al., 2009; Lomas

724   et al., 2010; Orchard et al., 2010; Sohm & Capone, 2010; Reynolds et al., 2014).

725

5. Conclusion

727   In this work we describe global patterns in surface ocean DOC:DON:DOP stoichiometry using

728   updated global ocean DOC, DON and DOP concentration datasets (Hansell et al., 2021; Liang et

729   al., 2022b). We find that bulk and labile surface ocean DOC:DON stoichiometry exhibit the least

730   spatial variability, consistent with prior work (Hansell & Carlson, 1998a, 2001; Bif et al., 2022),

731   although the labile DOC:DON stoichiometry is closer to the "Redfield" 6.6:1 C:N stoichiometry

732   (on average ~8.9:1) than bulk DOC:DON stoichiometry (on average ~14.6:1). Additionally,

733   significant differences in bulk and labile surface ocean DON:DOP and DOC:DOP stoichiometry

734   were observed within and among ocean basins, whether divided based on biogeochemical or

735   geographical boundaries, and we argue that these trends are driven by the significant rates of water

736   column denitrification occurring in the eastern tropical Pacific, and because of the high rates of

737   atmospheric dust deposition to the tropical North Atlantic. Specifically, we find that bulk and labile

738   surface ocean DON:DOP and DOC:DOP stoichiometry increase from the East to West in the

739   Pacific as a result of increasing pressure on the DOP pool as surface waters transit westwards in

740   the basin (Liang et al., 2022a). In the Atlantic, meridional increases in bulk and labile surface

741   ocean DON:DOP and DOC:DOP stoichiometry from the South to the North are coincident with

742   regions of low iron stress and high PO_4^{3-} stress, and the lowest concentrations of surface ocean

743   DOP observed globally. These observations illustrate the geochemical expression of subsurface

744 (i.e., denitrification) and atmospheric (dust deposition) processes on surface ocean organic matter
745 stoichiometry. We stress that these observations would not be possible without the considerable
746 effort associated with basin-crossing cruises including the CLIVAR, GO-SHIP, and
747 GEOTRACES field campaigns, which provide unique synoptic insight into global marine
748 biogeochemical processes.
749

750 **Data availability**
751 DOPv2021 database is publicly available at BCO DMO website (https://www.bco-
752 dmo.org/dataset/855139) and DOM data compilation is publicly available at NCEI
753 (https://doi.org/10.25921/s4f4-ye35)
754

760

761 **Author contributions**
762 ZL and ANK wrote the manuscript. ZL processed and analyzed the data. ZL, RTL, and ANK
763 designed the study. ZL, ANK and RTL revised the manuscript.
764

765 **Competing interests**
766 The authors declare that they have no conflict of interest.
767

768

769

770
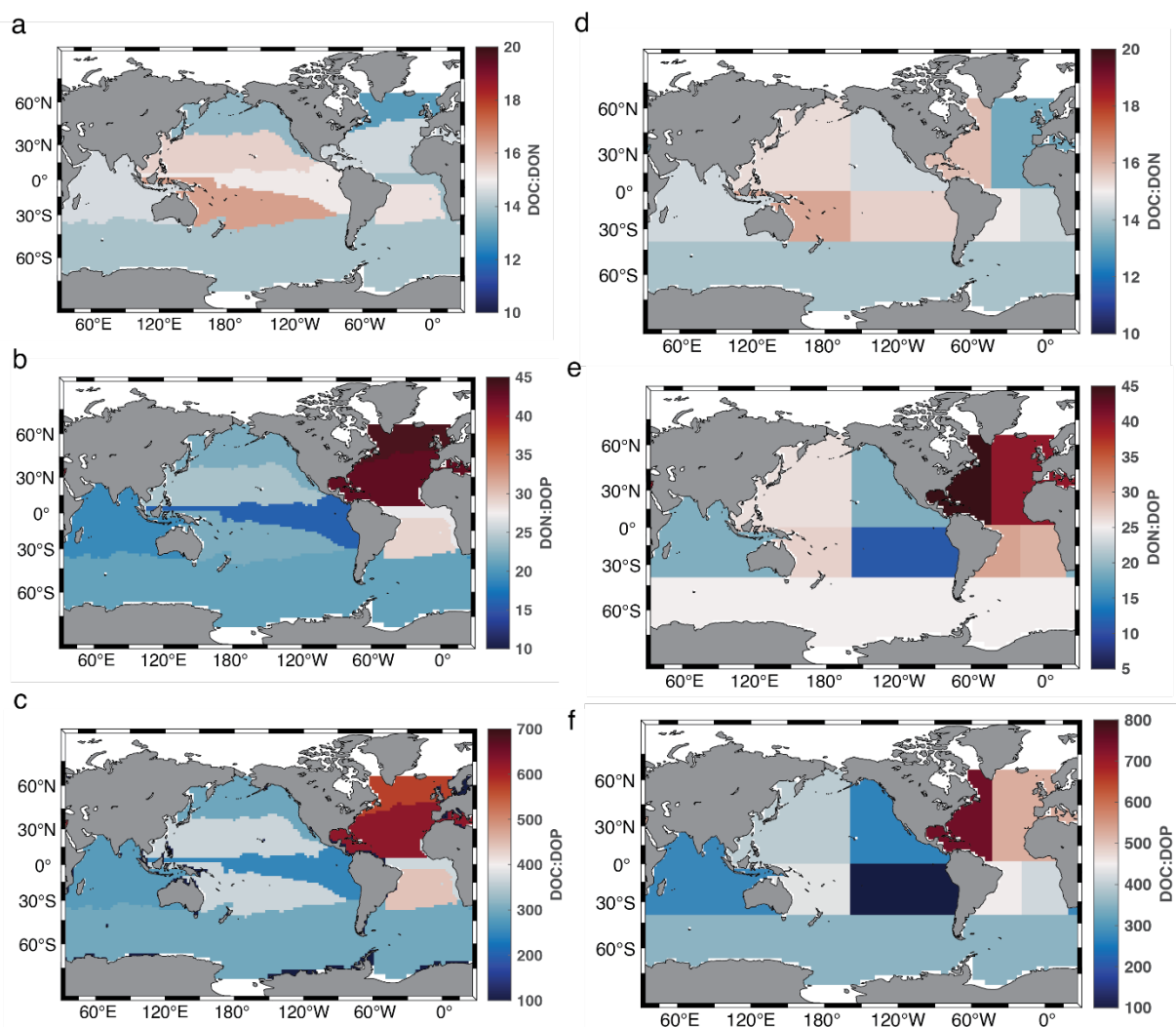
Figure 1. Surface (<73 m) ocean bulk DOC:DON (a), DON:DOP (b) and DOC:DOP (c) concentration ratios in different biogeochemical regions, and surface bulk DOC:DON (d), DON:DOP (e), and DOC:DOP (f) concentration ratios in different geographical regions.

774

775

776
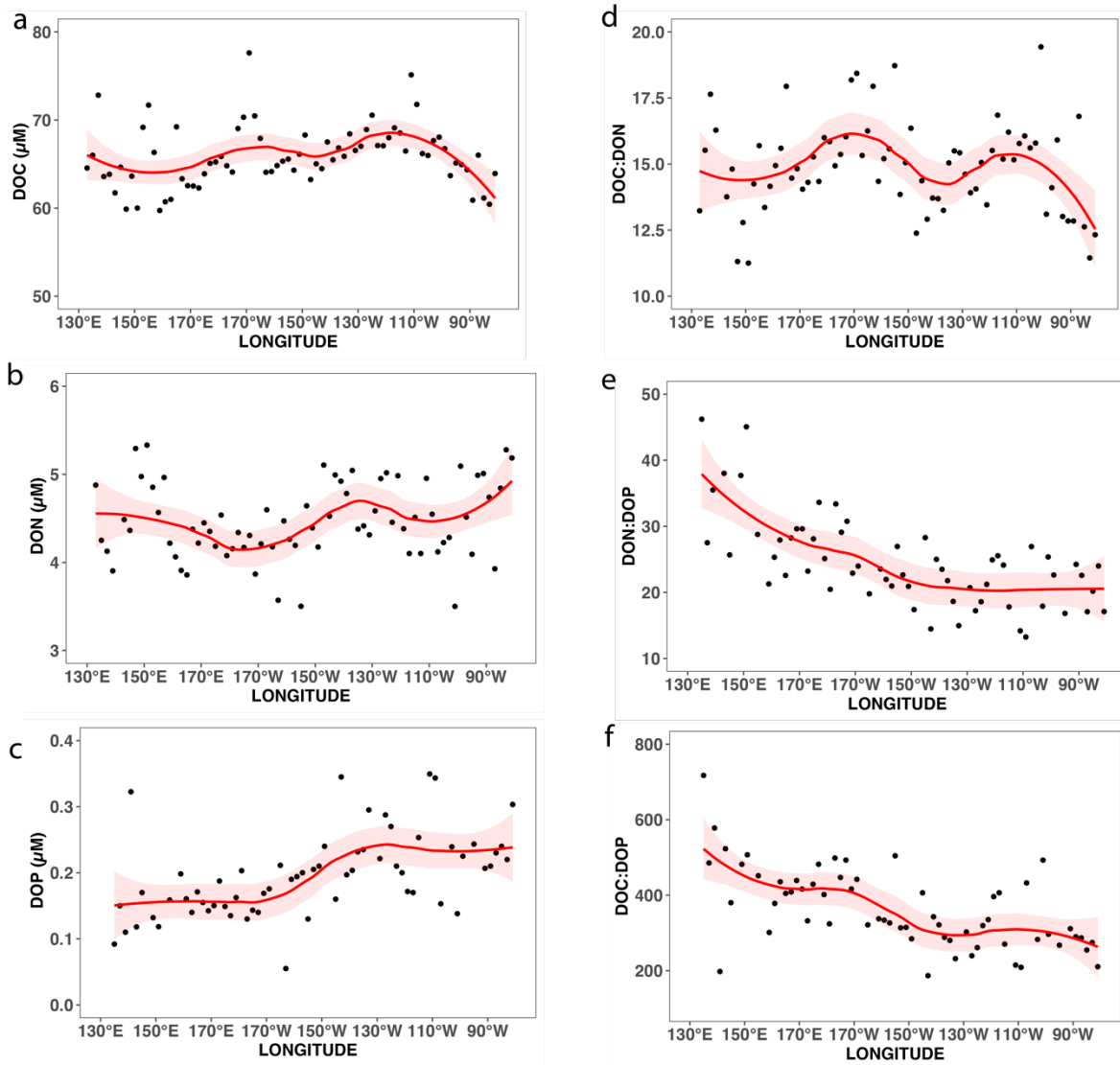
Figure 2. Combined North and South Pacific zonal mean surface (< 73 m) ocean bulk DOC (a),
DON (b), and DOP concentration (c), as well as bulk surface ocean DOC:DON (d), DON:DOP
(e) and DOC:DOP (f) concentration ratios. Red line shows the fitting curve of the data using the
LOWESS method (Cleveland, 1979) and red shading area shows the 95% confidence interval.

781
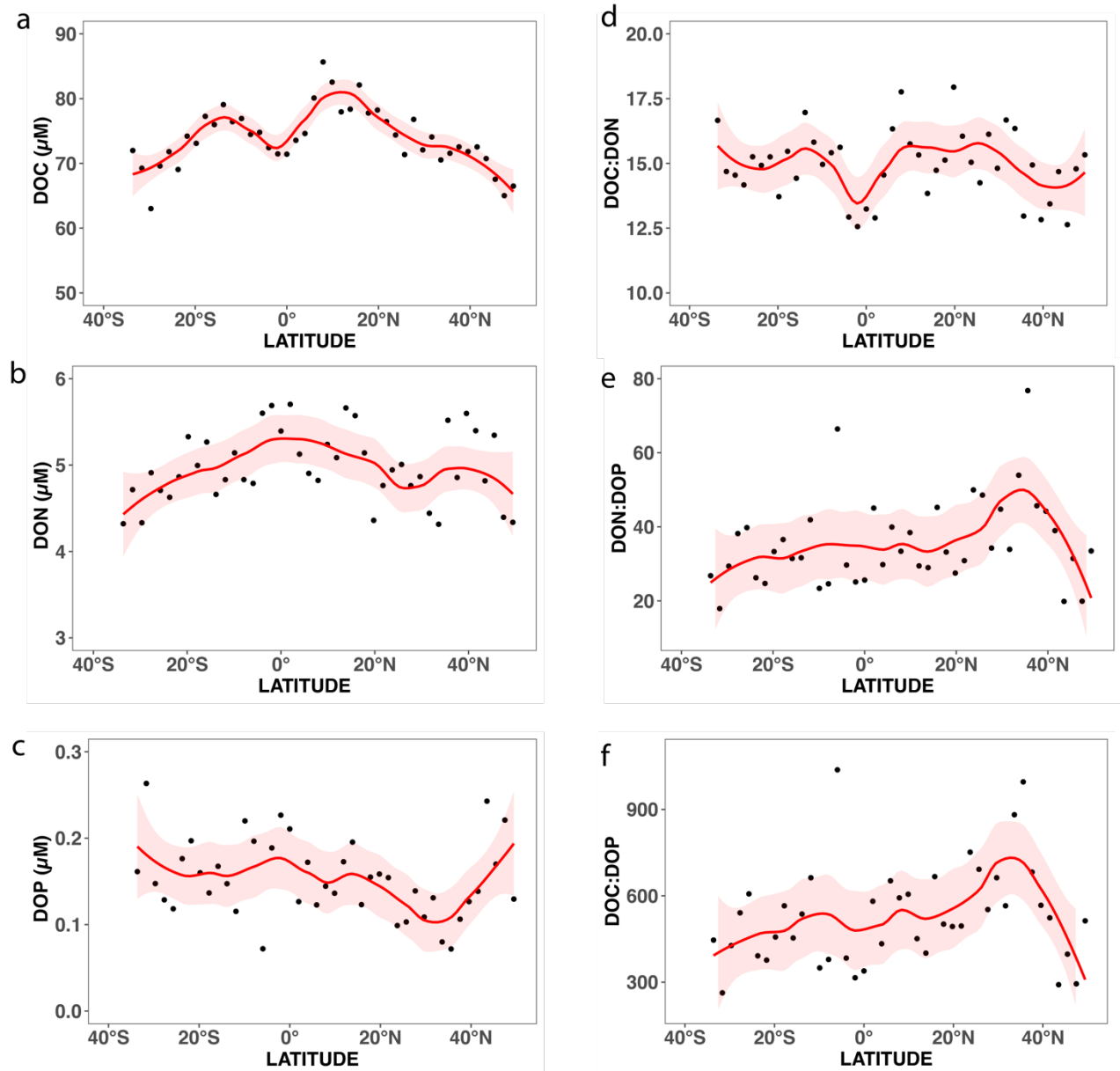
Figure 3. Combined West and East Atlantic mean meridional bulk surface ocean (<73 m) DOC (a), DON (b), and DOP (c), concentrations, as well as bulk surface ocean DOC:DON (d), DON:DOP (e), and DOC:DOP (f) concentration ratios. Red line shows the fitting curve of the data using the LOWESS method (Cleveland, 1979) and red shading area shows the 95% confidence interval.

a

b

c

788
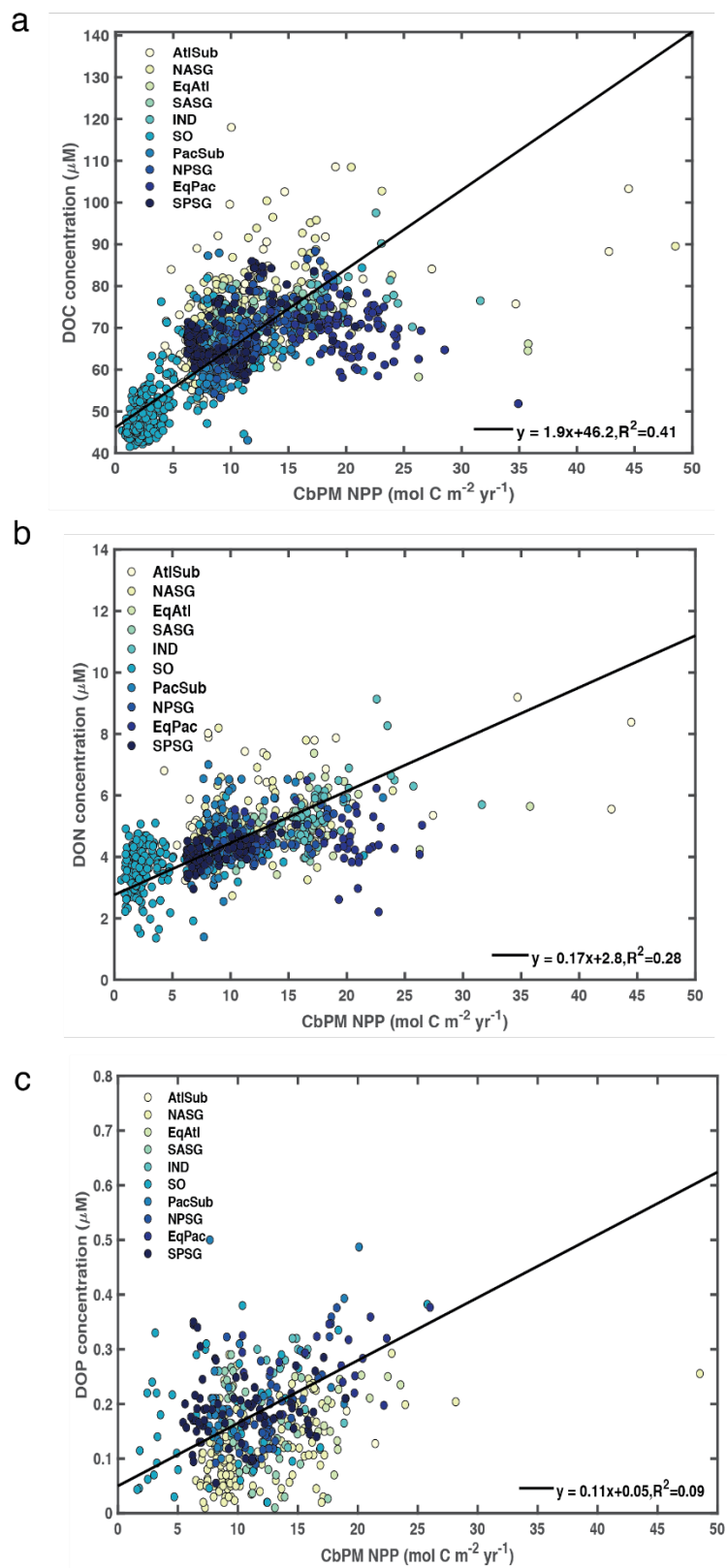
Figure 4. Type II linear regressions of bulk surface (<73 m) ocean DOC concentrations (a), DON concentrations (b), and DOP concentrations vs. Net Primary Productivity determined with the Carbon-based Productivity Model (CbPM) (Westberry et al., 2008). "AtlSub": Atlantic Subarctic region; "NASG": North Atlantic Subtropical Gyre; "EqAtl": Equatorial Atlantic region; "SASG": South Atlantic Subtropical Gyre; "IND": Indian Ocean; "SO": Southern Ocean; "PacSub": Pacific Subarctic region; "NPSG": North Pacific Subtropical Gyre; "EqPac": Equatorial Pacific region; "SPSG": South Pacific Subtropical Gyre.
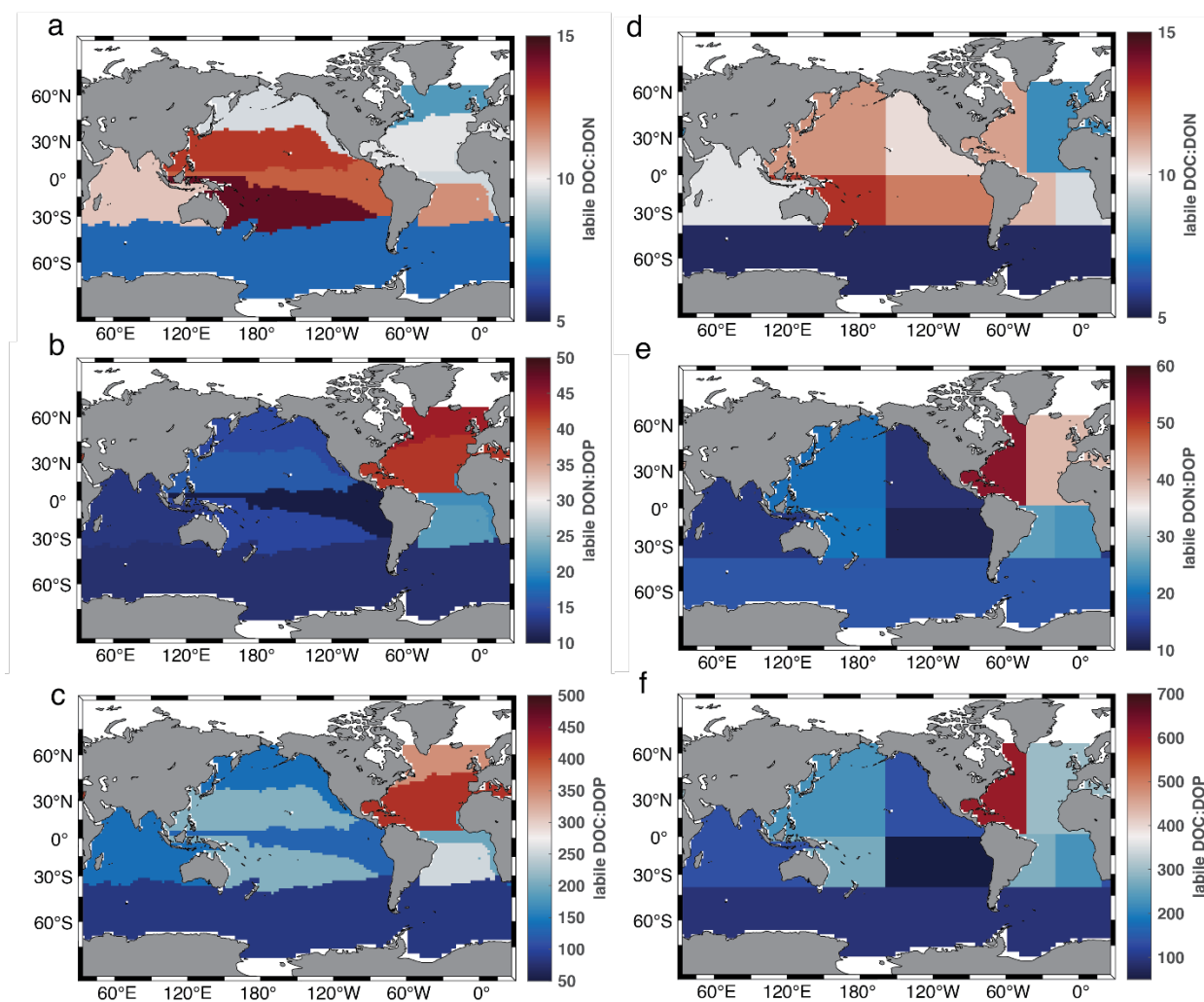
Figure 5. Labile surface (<73 m) ocean DOC:DON (a), DON:DOP (b), and DOC:DOP (c) concentration ratios in different biogeochemical regions, and labile surface ocean DOC:DON (d), DON:DOP (e), and DOC:DOP (f) concentration ratios in different geographical regions.
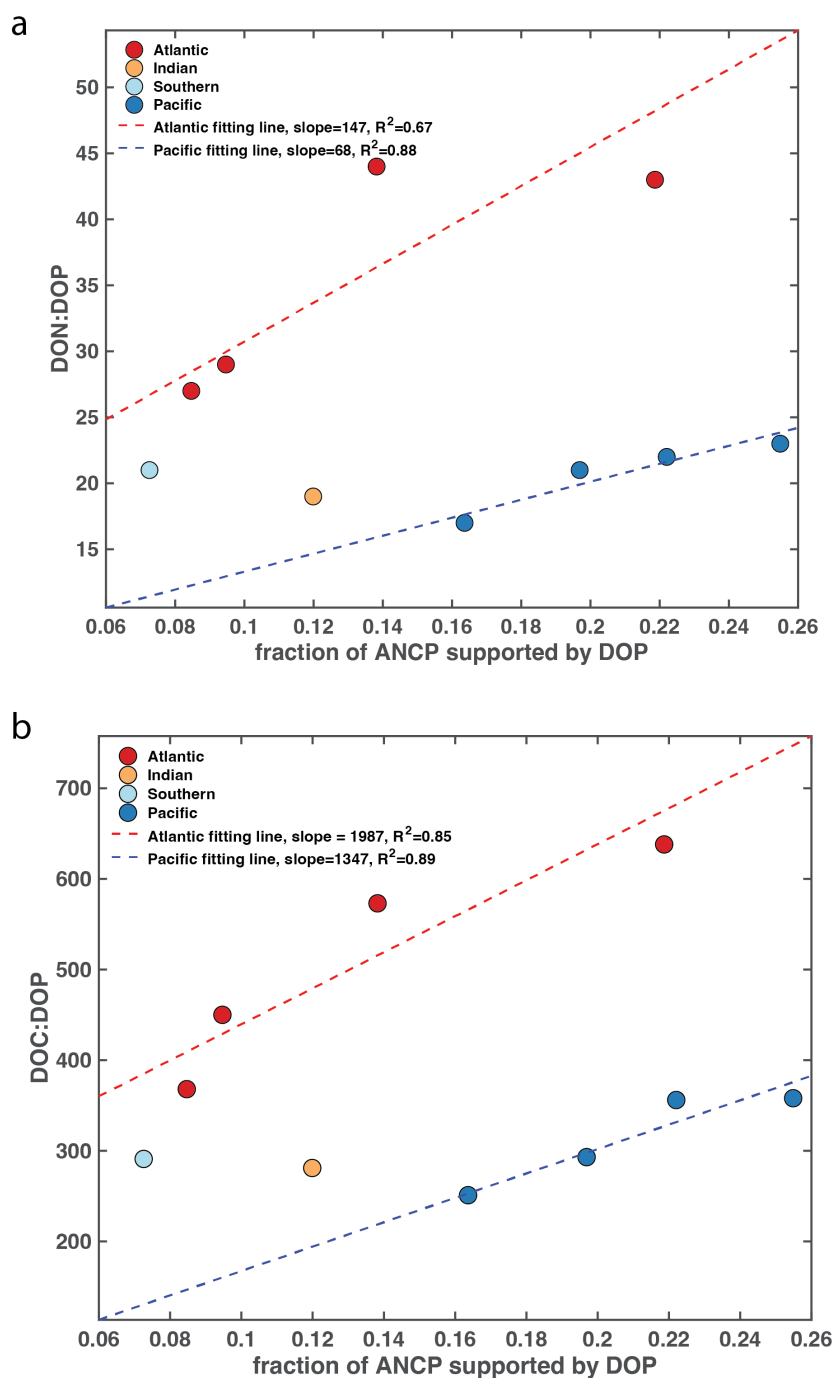
Figure 6. Correlations between bulk surface ocean DON:DOP (a) and DOC:DOP (b)
concentration ratios vs. the fraction of ANCP supported by DOP consumption. DON:DOP and
DOC:DOP concentration ratios are from Table 3 and are based on biogeochemical divisions.
Model-diagnosed fractions of ANCP supported by DOP consumption are from Letscher et al.,
2022.
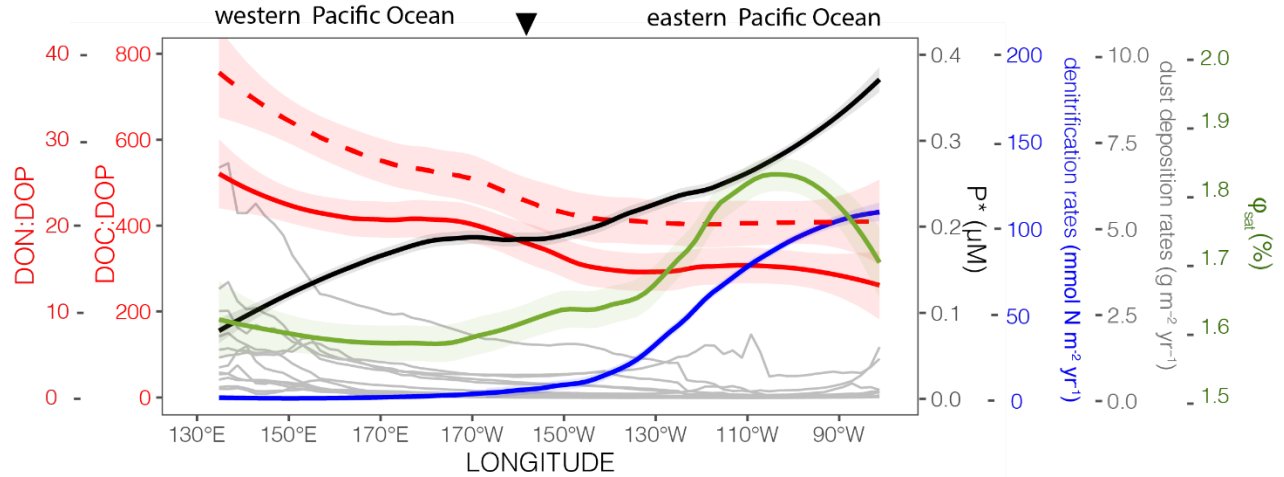
Figure 7. Combined North and South Pacific zonal mean bulk surface (< 73 m) ocean DOC:DOP concentration ratios (solid red line, same data as in Figure 2), DON:DOP concentration ratios (dashed red line, same data as in Figure 2), surface ocean P* (black line), water column denitrification rates (Wang et al., 2019) (blue line), NPQ-corrected φ_{sat} (green line), and dust deposition rates from 12 different model outputs (Xu & Weber, 2021)(gray lines). Shadings reflect the 95% confidence interval. Black inverted triangle represents 160° W.
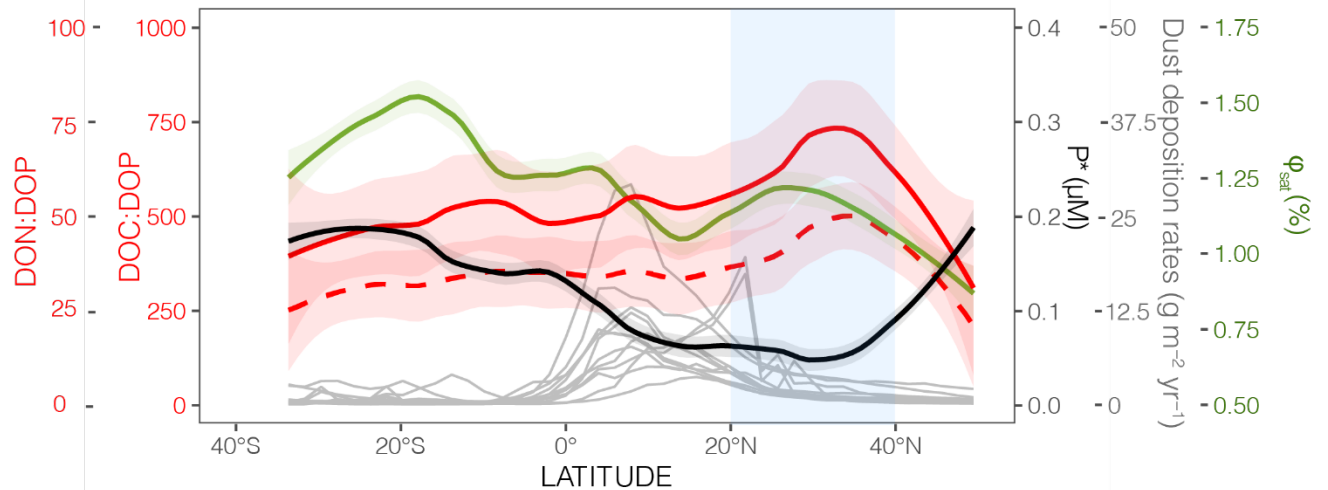
Figure 8. Combined Western and Eastern Atlantic meridional mean bulk surface (< 73 m) ocean DOC:DOP concentration ratios (solid red line, same data as in Figure 3), DON:DOP concentration ratios (dashed red line, same data as in Figure 3), surface ocean P* calculated from World Ocean Atlas 2013 (Garcia et al., 2013) (black line), NPQ-corrected φ_{sat} (Behrenfeld et al., 2009)(green line), and dust deposition rates from 12 different model outputs (Xu & Weber, 2021)(gray lines).

Blue shading marks the Sargasso Sea region (20˚ N – 40˚ N). Red, green, and black shadings

825 reflect the 95% confidence interval.

826

827
828 Figure 9. Comparison of surface ocean POM, labile, and bulk DOM stoichiometry in different

829 biogeochemical regions. The dashed line marks the canonical Redfield ratio (C:N:P = 106:16:1).

830 C:N:P ratios in POM were calculated from global ocean POM concentration datasets (Martiny et

831 al., 2014; Tanioka et al., 2022).

832
833

834   Table 1. Mean bulk surface (<73 m) ocean DOC, DON and DOP concentrations (±1 S.D.) in the

835   10 biogeochemical regions, where n_DOC, n_DON and n_DOP represent the number of DOC,

836   DON and DOP concentration observations in each region.

	DOC (µM)	n_DOC	DON (µM)	n_DON	DOP (µM)	n_DOP
AtlSub	68.7±15.4	313	5.3±1.7	94	0.12±0.04	11
NASG	70.2±8.6	493	4.8±0.9	244	0.11±0.07	229
EqAtl	73.5±21.6	46	5.3±1.1	43	0.20±0.07	26
SASG	67.5±6.3	130	4.4±0.7	126	0.15±0.07	89
IND	70.2±4.8	247	4.8±0.8	241	0.25±0.06	18
SO	52.4±8.3	569	3.7±0.8	349	0.18±0.09	67
PacSub	61.5±7.5	234	4.5±1.5	186	0.21±0.11	46
NPSG	68±6.3	228	4.4±0.4	151	0.19±0.08	93
EqPac	67.7±6.4	154	4.5±0.8	81	0.27±0.06	39
SPSG	67.7±6.8	228	4.2±0.5	171	0.19±0.06	141
Global mean	65.8	2642	4.5	1686	0.17	759

837

838   Table 2. Mean bulk surface (< 73 m) ocean DOC, DON and DOP concentrations (±1 S.D.) in the

839   10 geographical regions, where n_DOC, n_DON and n_DOP represent the number of DOC, DON

840   and DOP concentration observations in each region.

region	DOC (µM)	n_DOC	DON (µM)	n_DON	DOP (µM)	n_DOP
ENATL	67.0±10.2	586	5.1±1.3	206	0.13±0.07	162
WNATL	75.5±11.9	240	4.8±0.8	150	0.10±0.06	94
WSATL	70.1±11.4	89	4.6±0.9	85	0.15±0.07	71
ESATL	66.0±6.2	85	4.6±0.7	74	0.16±0.07	39
Indian	69.3±5.5	275	4.8±0.7	261	0.25±0.06	21
Southern	50.4±7.2	505	3.6±0.9	304	0.14±0.08	32
ENPAC	65.4±7.0	236	4.5±1.2	210	0.24±0.10	62
WNPAC	66.0±7.8	286	4.3±0.8	145	0.17±0.07	83
WSPAC	69.2±8.7	104	4.3±0.4	55	0.16±0.04	62
ESPAC	66.2±5.3	236	4.3±0.6	196	0.22±0.07	133
Global mean	65.8	2642	4.5	1686	0.17	759

841

842   Table 3. Mean (± 1 S.D.) bulk surface (< 73 m) ocean DOC:DON, DON:DOP, and DOC:DOP

843   concentration ratios in the 10 biogeochemical regions, calculated from Table 1.

Region	Mean DOC:DON	Mean DON:DOP	Mean DOC:DOP	Mean DOC:DON:DOP
AtlSub	13.0±5.1	44±20	573±230	573:44:1
NASG	14.6±3.3	43±29	638±414	638:43:1
EqAtl	13.9±5.0	27±11	368±168	368:27:1

SASG	15.3±2.8	29±14	450±214	450:29:1
IND	14.6±2.6	19±6	281±70	281:19:1
SO	14.2±3.8	21±12	291±153	291:21:1
PacSub	13.7±4.9	21±13	293±158	293:21:1
NPSG	15.5±2.0	23±10	358±154	358:23:1
EqPac	15.0±3.0	17±5	251±61	251:17:1
SPSG	16.1±2.5	22±7	356±118	356:22:1
Global mean	14.6	26	387	387:26:1

Table 4. Mean (± 1 S.D.) bulk surface (< 73 m) ocean DOC:DON, DON:DOP, and DOC:DOP concentration ratios in the 10 geographical regions, calculated from Table 2.

region	Mean DOC:DON	Mean DON:DOP	Mean DOC:DOP	Mean DOC:DON:DOP
ENATL	13.1±3.9	39±23	515±288	515:39:1
WNATL	15.7±3.6	48±30	755±468	755:48:1
WSATL	15.2±3.9	31±16	467±231	467:31:1
ESATL	14.3±2.6	29±13	413±185	413:29:1
Indian	14.4±2.4	19±5	277±70	277:19:1
Southern	14.0±4.0	26±16	360±212	360:26:1
ENPAC	14.5±4.2	19±9	273±117	273:19:1
WNPAC	15.3±3.4	25±11	388±166	388:25:1
WSPAC	16.1±2.5	27±7	433±121	433:27:1
ESPAC	15.4±2.5	20±7	301±99	301:20:1
Global mean	14.6	26	387	387:26:1

Table 5. Mean labile and refractory DOC:DON, DON:DOP, and DOC:DOP concentration ratios determined using different NPP data products and approaches. See text for details.

	DOC (µM)	DON (µM)	DOP (µM)	DOC:DON	DON:DOP	DOC:DOP	DOC:DON:DOP
Labile DOM (slope ratios, CbPM)				11.2:1	15.5:1	173:1	173:15.5:1
Labile DOM (slope ratios, VGPM)				10.7:1	16.4:1	176:1	176:16.4:1
Refractory DOM (intercept ratios, CbPM)	46	2.8	0.05	16.5:1	56:1	920:1	920:56:1
Refractory DOM (intercept ratios, VGPM)	45	2.5	0.05	18.0:1	50:1	900:1	900:50:1

Refractory DOM (>1000 m deep ocean average)	42	3.0	0.05	14.0:1	60:1	842:1	842:60:1

850

851

852   Table 6. Mean labile (± 1 S.D.) surface (< 73 m) ocean DOC, DON and DOP concentrations and

853   labile DOC:DON, DON:DOP and DOC:DOP concentration ratios in the 10 biogeochemical

854   regions.

region	laDOC (μM)	laDON (μM)	laDOP (μM)	laDOC:DON	laDON:DOP	laDOC:DOP	laDOC:DON:DOP
AtlSub	24.3±16.3	3.5±1.7	0.07±0.06	7.0±5.8	50±51	346±392	346:50:1
NASG	25.8±10.0	3.0±1.0	0.06±0.08	8.5±4.3	49±63	414±549	414:49:1
EqAtl	29.1±22.2	3.5±1.1	0.15±0.08	8.4±7.0	23±14	195±178	195:23:1
SASG	26.0±8.2	2.6±0.8	0.10±0.08	9.8±4.3	26±21	254±209	254:26:1
IND	27.8±7.1	3.0±0.9	0.20±0.07	9.2±3.6	15±7	138±58	138:15:1
SO	10.5±9.8	1.9±0.9	0.13±0.09	5.4±5.6	15±13	83±98	83:15:1
PacSub	22.0±9.1	2.7±1.5	0.16±0.11	8.1±5.8	17±15	139±114	139:17:1
NPSG	28.5±8.2	2.6±0.6	0.14±0.09	11.0±4.0	19±12	209±141	209:19:1
EqPac	28.2±8.2	2.7±0.9	0.22±0.07	10.6±4.7	12±5	127±53	127:12:1
SPSG	28.2±8.6	2.4±0.6	0.14±0.07	12.0±4.9	17±9	209±118	209:17:1
Global mean	25.0	2.8	0.14	8.9	20	179	179:20:1

855

856

857   Table 7. Mean (± 1 S.D.) labile surface (< 73 m) ocean DOC, DON, and DOP concentrations and

858   labile DOC:DON, DON:DOP and DOC:DOP concentration ratios in the 10 geographical

859   regions.

	laDOC (μM)	laDON (μM)	laDOP (μM)	laDOC:DON	laDON:DOP	laDOC:DOP	laDOC:DON:DOP
ENATL	23.5±11.8	3.3±1.3	0.08±0.09	7.1±4.6	42±51	299±372	299:42:1
WNATL	31.3±13.0	3.0±0.9	0.05±0.07	10.5±5.3	58±76	610±813	610:58:1
WSATL	28.8±12.6	2.8±1.0	0.10±0.08	10.1±5.7	27±22	276±236	276:27:1
ESATL	24.6±8.1	2.8±0.8	0.11±0.08	8.9±3.9	26±20	228±185	228:26:1
Indian	27.1±7.6	3.0±0.9	0.20±0.07	9.1±3.6	15±7	135±61	135:15:1
Southern	8.6±8.9	1.8±0.9	0.09±0.08	4.8±5.6	19±20	93±126	93:19:1
ENPAC	26.0±8.8	2.7±1.2	0.19±0.10	9.6±5.4	14±9	134±83	134:14:1
WNPAC	26.6±9.4	2.5±0.9	0.12±0.07	10.6±5.2	22±15	228±166	228:22:1
WSPAC	29.8±10.1	2.5±0.6	0.11±0.05	12.1±5.0	22±11	270±153	270:22:1
ESPAC	26.9±7.5	2.5±0.8	0.17±0.07	10.9±4.5	14±7	154±78	154:14:1
Global mean	25.0	2.8	0.14	8.9	20	179	179:20:1

860

References:

862   Anderson, L. G., & Amon, R. M. W. (2015). Chapter 14—DOM in the Arctic Ocean.

863   *Biogeochemistry of Marine Dissolved Organic Matter (Second Edition, eds.* D. A. Hansell

864   & C. A. Carlson *)* (pp. 609–633). Academic Press. https://doi.org/10.1016/B978-0-12-

865   405940-5.00014-5

866   Baker, A. R., Kelly, S. D., Biswas, K. F., Witt, M., & Jickells, T. D. (2003). Atmospheric deposition

867   of nutrients to the Atlantic Ocean. *Geophysical Research Letters*, *30*(24).

868   https://doi.org/10.1029/2003GL018518

869   Behrenfeld, M. J., & Falkowski, P. G. (1997). Photosynthetic rates derived from satellite-based

870   chlorophyll concentration. *Limnology and Oceanography*, *42*(1), 1–20.

871   https://doi.org/10.4319/lo.1997.42.1.0001

872   Behrenfeld, M. J., & Milligan, A. J. (2013). Photophysiological Expressions of Iron Stress in

873   Phytoplankton. *Annual Review of Marine Science*, *5*(1), 217–246.

874   https://doi.org/10.1146/annurev-marine-121211-172356

875   Behrenfeld, M. J., Westberry, T. K., Boss, E. S., O'Malley, R. T., Siegel, D. A., Wiggert, J. D., Franz,

876   B. A., McClain, C. R., Feldman, G. C., Doney, S. C., Moore, J. K., Dall'Olmo, G., Milligan, A.

877   J., Lima, I., & Mahowald, N. (2009). Satellite-detected fluorescence reveals global

878   physiology of ocean phytoplankton. *Biogeosciences*, *6*(5), 779–794.

879   https://doi.org/10.5194/bg-6-779-2009

880   Benner, R., Louchouarn, P., & Amon, R. M. W. (2005). Terrigenous dissolved organic matter in

881   the Arctic Ocean and its transport to surface and deep waters of the North Atlantic.

882   *Global Biogeochemical Cycles*, *19*(2). https://doi.org/10.1029/2004GB002398

883   Berges, J. A., & Mulholland, M. R. (2008). Chapter 32—Enzymes and Nitrogen Cycling. *Nitrogen*

884   *in the Marine Environment (Second Edition, eds.* D. G. Capone, D. A. Bronk, M. R.

885   Mulholland, & E. J. Carpenter*)* (pp. 1385–1444). Academic Press.

886   https://doi.org/10.1016/B978-0-12-372522-6.00032-3

887   Bif, M. B., Bourbonnais, A., Hansell, D. A., Granger, J., Westbrook, H., & Altabet, M. A. (2022).

888   Controls on surface distributions of dissolved organic carbon and nitrogen in the

889   southeast Pacific Ocean. *Marine Chemistry*, *244*, 104136.

890   https://doi.org/10.1016/j.marchem.2022.104136

891   Björkman, K. M., & Karl, D. M. (2003). Bioavailability of dissolved organic phosphorus in the

892   euphotic zone at Station ALOHA, North Pacific Subtropical Gyre. *Limnology and*

893   *Oceanography*, *48*(3), 1049–1057. https://doi.org/10.4319/lo.2003.48.3.1049

894   Bronk, D. A., See, J. H., Bradley, P., & Killberg, L. (2007). DON as a source of bioavailable

895   nitrogen for phytoplankton. *Biogeosciences*, *4*(3), 283–296. https://doi.org/10.5194/bg-

896   4-283-2007

897   Browning, T. J., Bouman, H. A., & Moore, C. M. (2014). Satellite-detected fluorescence:

898   Decoupling nonphotochemical quenching from iron stress signals in the South Atlantic

899   and Southern Ocean. *Global Biogeochemical Cycles*, *28*(5), 510–524.

900   https://doi.org/10.1002/2013GB004773

901　Carlson, C. A., Ducklow, H. W., & Michaels, A. F. (1994). Annual flux of dissolved organic carbon

902　　　from the euphotic zone in the northwestern Sargasso Sea. *Nature*, *371*(6496), 405–408.

903　　　https://doi.org/10.1038/371405a0

904　Carlson, C. A., & Hansell, D. A. (2015). Chapter 3—DOM Sources, Sinks, Reactivity, and Budgets.

905　　　*Biogeochemistry of Marine Dissolved Organic Matter (Second Edition, eds.* D. A. Hansell

906　　　& C. A. Carlson*)* (pp. 65–126). Academic Press. https://doi.org/10.1016/B978-0-12-

907　　　405940-5.00003-0

908　Carr, M.-E., Friedrichs, M. A. M., Schmeltz, M., Noguchi Aita, M., Antoine, D., Arrigo, K. R.,

909　　　Asanuma, I., Aumont, O., Barber, R., Behrenfeld, M., Bidigare, R., Buitenhuis, E. T.,

910　　　Campbell, J., Ciotti, A., Dierssen, H., Dowell, M., Dunne, J., Esaias, W., Gentili, B., …

911　　　Yamanaka, Y. (2006). A comparison of global estimates of marine primary production

912　　　from ocean color. *Deep Sea Research Part II: Topical Studies in Oceanography*, *53*(5),

913　　　741–770. https://doi.org/10.1016/j.dsr2.2006.01.028

914　Chang, B. X., Devol, A. H., & Emerson, S. R. (2010). Denitrification and the nitrogen gas excess in

915　　　the eastern tropical South Pacific oxygen deficient zone. *Deep Sea Research Part I:*

916　　　*Oceanographic Research Papers*, *57*(9), 1092–1101.

917　　　https://doi.org/10.1016/j.dsr.2010.05.009

918　Chang, B. X., Devol, A. H., & Emerson, S. R. (2012). Fixed nitrogen loss from the eastern tropical

919　　　North Pacific and Arabian Sea oxygen deficient zones determined from measurements

920　　　of N2:Ar. *Global Biogeochemical Cycles*, *26*(3). https://doi.org/10.1029/2011GB004207

921   Cleveland, W. S. (1979). Robust Locally Weighted Regression and Smoothing Scatterplots.

922   *Journal of the American Statistical Association*, *74*(368), 829–836.

923   https://doi.org/10.1080/01621459.1979.10481038

924   Connolly, C. T., Cardenas, M. B., Burkart, G. A., Spencer, R. G. M., & McClelland, J. W. (2020).

925   Groundwater as a major source of dissolved organic matter to Arctic coastal waters.

926   *Nature Communications*, *11*(1), 1479. https://doi.org/10.1038/s41467-020-15250-8

927   Deutsch, C., Sarmiento, J. L., Sigman, D. M., Gruber, N., & Dunne, J. P. (2007). Spatial coupling of

928   nitrogen inputs and losses in the ocean. *Nature*, *445*(7124), 163–167.

929   https://doi.org/10.1038/nature05392

930   DeVries, T. (2022). The Ocean Carbon Cycle. *Annual Review of Environment and Resources*,

931   *47*(1), 317–341. https://doi.org/10.1146/annurev-environ-120920-111307

932   DeVries, T., & Deutsch, C. (2014). Large-scale variations in the stoichiometry of marine organic

933   matter respiration. *Nature Geoscience*, *7*(12), 890–894.

934   https://doi.org/10.1038/ngeo2300

935   DeVries, T., Deutsch, C., Primeau, F., Chang, B., & Devol, A. (2012). Global rates of water-column

936   denitrification derived from nitrogen gas measurements. *Nature Geoscience*, *5*(8), 547–

937   550. https://doi.org/10.1038/ngeo1515

938   DeVries, T., & Holzer, M. (2019). Radiocarbon and Helium Isotope Constraints on Deep Ocean

939   Ventilation and Mantle-3He Sources. *Journal of Geophysical Research: Oceans*, *124*(5),

940   3036–3057. https://doi.org/10.1029/2018JC014716

941   DeVries, T., & Weber, T. (2017). The export and fate of organic matter in the ocean: New

942   constraints from combining satellite and oceanographic tracer observations. *Global*

943   *Biogeochemical Cycles*, *31*(3), 535–555. https://doi.org/10.1002/2016GB005551

944   Duhamel, S., Diaz, J. M., Adams, J. C., Djaoudi, K., Steck, V., & Waggoner, E. M. (2021).

945   Phosphorus as an integral component of global marine biogeochemistry. *Nature*

946   *Geoscience*, *14*(6), 359–368. https://doi.org/10.1038/s41561-021-00755-8

947   Dyhrman, S. T., Chappell, P. D., Haley, S. T., Moffett, J. W., Orchard, E. D., Waterbury, J. B., &

948   Webb, E. A. (2006). Phosphonate utilization by the globally important marine diazotroph

949   Trichodesmium. *Nature*, *439*(7072), 68–71. https://doi.org/10.1038/nature04203

950   Emerson, S. (2014). Annual net community production and the biological carbon flux in the

951   ocean. *Global Biogeochemical Cycles*, *28*(1), 14–28.

952   https://doi.org/10.1002/2013GB004680

953   Foreman, R. K., Björkman, K. M., Carlson, C. A., Opalk, K., & Karl, D. M. (2019). Improved

954   ultraviolet photo-oxidation system yields estimates for deep-sea dissolved organic

955   nitrogen and phosphorus. *Limnology and Oceanography: Methods*, *17*(4), 277–291.

956   https://doi.org/10.1002/lom3.10312

957   Galbraith, E. D., & Martiny, A. C. (2015). A simple nutrient-dependence mechanism for

958   predicting the stoichiometry of marine ecosystems. *Proceedings of the National*

959   *Academy of Sciences*, *112*(27), 8199–8204. https://doi.org/10.1073/pnas.1423917112

960   Garcia, H. E., Locarnini, R. A., Boyer, T. P., Antonov, J. I., Baranova, O. K., Zweng, M. M., Reagan,

961   J. R., & Johnson, D. R. (2013). *World Ocean Atlas 2013, Volume 4: Dissolved Inorganic*

962   *Nutrients (phosphate, nitrate, silicate). S. Levitus, Ed., A. Mishonov Technical Ed.; NOAA*

963   *Atlas NESDIS 76, 25 pp.* https://repository.library.noaa.gov/view/noaa/14850

964   Gledhill, M., Hollister, A., Seidel, M., Zhu, K., Achterberg, E. P., Dittmar, T., & Koschinsky, A.

965   (2022). Trace metal stoichiometry of dissolved organic matter in the Amazon plume.

966   *Science Advances*, *8*(31), eabm2249. https://doi.org/10.1126/sciadv.abm2249

967   Gruber, N., Keeling, C. D., & Stocker, T. F. (1998). Carbon-13 constraints on the seasonal

968   inorganic carbon budget at the BATS site in the northwestern Sargasso Sea. *Deep Sea*

969   *Research Part I: Oceanographic Research Papers*, *45*(4), 673–717.

970   https://doi.org/10.1016/S0967-0637(97)00098-8

971   Guieu, C., Bonnet, S., Petrenko, A., Menkes, C., Chavagnac, V., Desboeufs, K., Maes, C., &

972   Moutin, T. (2018). Iron from a submarine source impacts the productive layer of the

973   Western Tropical South Pacific (WTSP). *Scientific Reports*, *8*(1), 9075.

974   https://doi.org/10.1038/s41598-018-27407-z

975   Hain, M. P., Sigman, D. M., & Haug, G. H. (2014). The Biological Pump in the Past. *Treatise on*

976   *Geochemistry (Second Edition, eds.* H. D. Holland & K. K. Turekian *)* (pp. 485–517).

977   Elsevier. https://doi.org/10.1016/B978-0-08-095975-7.00618-5

978   Hansell, D. A., & Carlson, C. A. (1998a). Net community production of dissolved organic carbon.

979   *Global Biogeochemical Cycles*, *12*(3), 443–453. https://doi.org/10.1029/98GB01928

980   Hansell, D. A., & Carlson, C. A. (1998b). Deep-ocean gradients in the concentration of dissolved

981   organic carbon. *Nature*, *395*(6699), 263–266. https://doi.org/10.1038/26200

982   Hansell, D. A., & Carlson, C. A. (2001). Biogeochemistry of total organic carbon and nitrogen in

983   the Sargasso Sea: Control by convective overturn. *Deep Sea Research Part II: Topical*

984 *Studies in Oceanography*, *48*(8), 1649–1667. https://doi.org/10.1016/S0967-

985 0645(00)00153-3

986 Hansell, D. A., Carlson, C. A., Amon, R. M. W., Álvarez-Salgado, X. A., Yamashita, Y., Romera-

987 Castillo, C., & Bif, M. B. (2021). Compilation of dissolved organic matter (DOM) data

988 obtained from global ocean observations from 1994 to 2020 (NCEI Accession 0227166).

989 *NOAA National Centers for Environmental Information*. https://doi.org/10.25921/s4f4-

990 ye35

991 Hansell, D. A., Carlson, C. A., Repeta, D. J., & Schlitzer, R. (2009). Dissolved Organic Matter in the

992 Ocean: A Controversy Stimulates New Insights. *Oceanography*, *22*(4), 202–211.

993 Hansell, D. A., Kadko, D., & Bates, N. R. (2004). Degradation of Terrigenous Dissolved Organic

994 Carbon in the Western Arctic Ocean. *Science*, *304*(5672), 858–861.

995 https://doi.org/10.1126/science.1096175

996 Hashihama, F., Saito, H., Shiozaki, T., Ehama, M., Suwa, S., Sugiyama, T., Kato, H., Kanda, J.,

997 Sato, M., Kodama, T., Yamaguchi, T., Horii, S., Tanita, I., Takino, S., Takahashi, K., Ogawa,

998 H., Boyd, P. W., & Furuya, K. (2020). Biogeochemical Controls of Particulate Phosphorus

999 Distribution Across the Oligotrophic Subtropical Pacific Ocean. *Global Biogeochemical*

1000 *Cycles*, *34*(9), e2020GB006669. https://doi.org/10.1029/2020GB006669

1001 Hopkinson, C. S., & Vallino, J. J. (2005). Efficient export of carbon to the deep ocean through

1002 dissolved organic matter. *Nature*, *433*(7022), 142–145.

1003 https://doi.org/10.1038/nature03191

1004 Hopwood, M. J., Carroll, D., Browning, T. J., Meire, L., Mortensen, J., Krisch, S., & Achterberg, E.

1005 P. (2018). Non-linear response of summertime marine productivity to increased

1006 meltwater discharge around Greenland. *Nature Communications*, *9*(1), 3256.

1007 https://doi.org/10.1038/s41467-018-05488-8

1008 Inomura, K., Deutsch, C., Jahn, O., Dutkiewicz, S., & Follows, M. J. (2022). Global patterns in

1009 marine organic matter stoichiometry driven by phytoplankton ecophysiology. *Nature*

1010 *Geoscience*, *15*(12), 1034–1040. https://doi.org/10.1038/s41561-022-01066-2

1011 Jickells, T., & Moore, C. M. (2015). The Importance of Atmospheric Deposition for Ocean

1012 Productivity. *Annual Review of Ecology, Evolution, and Systematics*, *46*(1), 481–501.

1013 https://doi.org/10.1146/annurev-ecolsys-112414-054118

1014 John, S. G., Liang, H., Weber, T., DeVries, T., Primeau, F., Moore, K., Holzer, M., Mahowald, N.,

1015 Gardner, W., Mishonov, A., Richardson, M. J., Faugere, Y., & Taburet, G. (2020).

1016 AWESOME OCIM: A simple, flexible, and powerful tool for modeling elemental cycling in

1017 the oceans. *Chemical Geology*, *533*, 119403.

1018 https://doi.org/10.1016/j.chemgeo.2019.119403

1019 Johnson, K. S., Riser, S. C., & Karl, D. M. (2010). Nitrate supply from deep to near-surface waters

1020 of the North Pacific subtropical gyre. *Nature*, *465*(7301), 1062–1065.

1021 https://doi.org/10.1038/nature09170

1022 Kadko, D., & Johns, W. (2011). Inferring upwelling rates in the equatorial Atlantic using 7Be

1023 measurements in the upper ocean. *Deep Sea Research Part I: Oceanographic Research*

1024 *Papers*, *58*(6), 647–657. https://doi.org/10.1016/j.dsr.2011.03.004

1025 Kathuria, S., & Martiny, A. C. (2011). Prevalence of a calcium-based alkaline phosphatase

1026 associated with the marine cyanobacterium Prochlorococcus and other ocean bacteria.

1027   *Environmental Microbiology*, *13*(1), 74–83. https://doi.org/10.1111/j.1462-

1028   2920.2010.02310.x

1029   Keeling, C. D., Brix, H., & Gruber, N. (2004). Seasonal and long-term dynamics of the upper

1030   ocean carbon cycle at Station ALOHA near Hawaii. *Global Biogeochemical Cycles*, *18*(4).

1031   https://doi.org/10.1029/2004GB002227

1032   Knapp, A. N., Casciotti, K. L., Berelson, W. M., Prokopenko, M. G., & Capone, D. G. (2016). Low

1033   rates of nitrogen fixation in eastern tropical South Pacific surface waters. *Proceedings of*

1034   *the National Academy of Sciences*, *113*(16), 4398–4403.

1035   https://doi.org/10.1073/pnas.1515641113

1036   Knapp, A. N., Casciotti, K. L., & Prokopenko, M. G. (2018a). Dissolved Organic Nitrogen

1037   Production and Consumption in Eastern Tropical South Pacific Surface Waters. *Global*

1038   *Biogeochemical Cycles*, *32*(5), 769–783. https://doi.org/10.1029/2017GB005875

1039   Knapp, A. N., Hastings, M. G., Sigman, D. M., Lipschultz, F., & Galloway, J. N. (2010). The flux

1040   and isotopic composition of reduced and total nitrogen in Bermuda rain. *Marine*

1041   *Chemistry*, *120*(1), 83–89. https://doi.org/10.1016/j.marchem.2008.08.007

1042   Knapp, A. N., McCabe, K. M., Grosso, O., Leblond, N., Moutin, T., & Bonnet, S. (2018b).

1043   Distribution and rates of nitrogen fixation in the western tropical South Pacific Ocean

1044   constrained by nitrogen isotope budgets. *Biogeosciences*, *15*(9), 2619–2628.

1045   https://doi.org/10.5194/bg-15-2619-2018

1046   Knapp, A. N., Thomas, R. K., Stukel, M. R., Kelly, T. B., Landry, M. R., Selph, K. E., Malca, E.,

1047   Gerard, T., & Lamkin, J. (2021). Constraining the sources of nitrogen fueling export

1048   production in the Gulf of Mexico using nitrogen isotope budgets. *Journal of Plankton*

1049   *Research*, *44*(5), 692–710. https://doi.org/10.1093/plankt/fbab049

1050 Lang, S. Q., Butterfield, D. A., Lilley, M. D., Paul Johnson, H., & Hedges, J. I. (2006). Dissolved

1051   organic carbon in ridge-axis and ridge-flank hydrothermal systems. *Geochimica et*

1052   *Cosmochimica Acta*, *70*(15), 3830–3842. https://doi.org/10.1016/j.gca.2006.04.031

1053 Lee, J. A., Garcia, C. A., Larkin, A. A., Carter, B. R., & Martiny, A. C. (2021). Linking a Latitudinal

1054   Gradient in Ocean Hydrography and Elemental Stoichiometry in the Eastern Pacific

1055   Ocean. *Global Biogeochemical Cycles*, *35*(5), e2020GB006622.

1056   https://doi.org/10.1029/2020GB006622

1057 Letscher, R., Primeau, F., & Moore, J. (2016). Nutrient budgets in the subtropical ocean gyres

1058   dominated by lateral transport. *Nature Geoscience*, *9*.

1059   https://doi.org/10.1038/NGEO2812

1060 Letscher, R. T., Hansell, D. A., Carlson, C. A., Lumpkin, R., & Knapp, A. N. (2013). Dissolved

1061   organic nitrogen in the global surface ocean: Distribution and fate. *Global*

1062   *Biogeochemical Cycles*, *27*(1), 141–153. https://doi.org/10.1029/2012GB004449

1063 Letscher, R. T., & Moore, J. K. (2015). Preferential remineralization of dissolved organic

1064   phosphorus and non-Redfield DOM dynamics in the global ocean: Impacts on marine

1065   productivity, nitrogen fixation, and carbon export. *Global Biogeochemical Cycles*, *29*(3),

1066   325–340. https://doi.org/10.1002/2014GB004904

1067 Letscher, R. T., Moore, J. K., Teng, Y.-C., & Primeau, F. (2015). Variable C: N : P stoichiometry of

1068   dissolved organic matter cycling in the Community Earth System Model. *Biogeosciences*,

1069   *12*(1), 209–221. https://doi.org/10.5194/bg-12-209-2015

1070 Letscher, R. T., Wang, W.-L., Liang, Z., & Knapp, A. N. (2022). Regionally Variable Contribution of

1071 Dissolved Organic Phosphorus to Marine Annual Net Community Production. *Global

1072 Biogeochemical Cycles*, *36*(12), e2022GB007354.

1073 https://doi.org/10.1029/2022GB007354

1074 Li, T., Guo, C., Zhang, Y., Wang, C., Lin, X., & Lin, S. (2018). Identification and Expression Analysis

1075 of an Atypical Alkaline Phosphatase in Emiliania huxleyi. *Frontiers in Microbiology*, *9*.

1076 https://doi.org/10.3389/fmicb.2018.02156

1077 Liang, Z., Letscher, R. T., & Knapp, A. N. (2022a). Dissolved organic phosphorus concentrations

1078 in the surface ocean controlled by both phosphate and iron stress. *Nature Geoscience*,

1079 *15*(8), 651–657. https://doi.org/10.1038/s41561-022-00988-1

1080 Liang, Z., McCabe, K., Fawcett, S. E., Forrer, H. J., Hashihama, F., Jeandel, C., Marconi, D.,

1081 Planquette, H., Saito, M. A., Sohm, J. A., Thomas, R. K., Letscher, R. T., & Knapp, A. N.

1082 (2022b). A global ocean dissolved organic phosphorus concentration database

1083 (DOPv2021). *Scientific Data*, *9*(1), 772. https://doi.org/10.1038/s41597-022-01873-7

1084 Lomas, M. W., Burke, A. L., Lomas, D. A., Bell, D. W., Shen, C., Dyhrman, S. T., & Ammerman, J.

1085 W. (2010). Sargasso Sea phosphorus biogeochemistry: An important role for dissolved

1086 organic phosphorus (DOP). *Biogeosciences*, *7*(2), 695–710. https://doi.org/10.5194/bg-

1087 7-695-2010

1088 Lønborg, C., Álvarez–Salgado, X. A., Letscher, R. T., & Hansell, D. A. (2018). Large Stimulation of

1089 Recalcitrant Dissolved Organic Carbon Degradation by Increasing Ocean Temperatures.

1090 *Frontiers in Marine Science*, *4*.

1091 https://www.frontiersin.org/articles/10.3389/fmars.2017.00436

1092   Mahadevan, A. (2016). The Impact of Submesoscale Physics on Primary Productivity of

1093   Plankton. *Annual Review of Marine Science*, *8*(1), 161–184.

1094   https://doi.org/10.1146/annurev-marine-010814-015912

1095   Mahowald, N. M., Baker, A. R., Bergametti, G., Brooks, N., Duce, R. A., Jickells, T. D., Kubilay, N.,

1096   Prospero, J. M., & Tegen, I. (2005). Atmospheric global dust cycle and iron inputs to the

1097   ocean. *Global Biogeochemical Cycles*, *19*(4). https://doi.org/10.1029/2004GB002402

1098   Martiny, A. C., Pham, C. T. A., Primeau, F. W., Vrugt, J. A., Moore, J. K., Levin, S. A., & Lomas, M.

1099   W. (2013). Strong latitudinal patterns in the elemental ratios of marine plankton and

1100   organic matter. *Nature Geoscience*, *6*(4), 279–283. https://doi.org/10.1038/ngeo1757

1101   Martiny, A. C., Vrugt, J. A., & Lomas, M. W. (2014). Concentrations and ratios of particulate

1102   organic carbon, nitrogen, and phosphorus in the global ocean. *Scientific Data*, *1*(1),

1103   140048. https://doi.org/10.1038/sdata.2014.48

1104   Mather, R. L., Reynolds, S. E., Wolff, G. A., Williams, R. G., Torres-Valdes, S., Woodward, E. M.

1105   S., Landolfi, A., Pan, X., Sanders, R., & Achterberg, E. P. (2008). Phosphorus cycling in the

1106   North and South Atlantic Ocean subtropical gyres. *Nature Geoscience*, *1*(7), 439–443.

1107   https://doi.org/10.1038/ngeo232

1108   McCarthy, M. D., Benner, R., Lee, C., Hedges, J. I., & Fogel, M. L. (2004). Amino acid carbon

1109   isotopic fractionation patterns in oceanic dissolved organic matter: An unaltered

1110   photoautotrophic source for dissolved organic nitrogen in the ocean? *Marine Chemistry*,

1111   *92*(1), 123–134. https://doi.org/10.1016/j.marchem.2004.06.021

1112   Medeiros, P. M., Seidel, M., Ward, N. D., Carpenter, E. J., Gomes, H. R., Niggemann, J., Krusche,

1113   A. V., Richey, J. E., Yager, P. L., & Dittmar, T. (2015). Fate of the Amazon River dissolved

1114   organic matter in the tropical Atlantic Ocean. *Global Biogeochemical Cycles*, *29*(5), 677–

1115   690. https://doi.org/10.1002/2015GB005115

1116 Moore, C. M., Mills, M. M., Arrigo, K. R., Berman-Frank, I., Bopp, L., Boyd, P. W., Galbraith, E. D.,

1117   Geider, R. J., Guieu, C., Jaccard, S. L., Jickells, T. D., La Roche, J., Lenton, T. M.,

1118   Mahowald, N. M., Marañón, E., Marinov, I., Moore, J. K., Nakatsuka, T., Oschlies, A., …

1119   Ulloa, O. (2013). Processes and patterns of oceanic nutrient limitation. *Nature*

1120   *Geoscience*, *6*(9), 701–710. https://doi.org/10.1038/ngeo1765

1121 Mopper, K., Kieber, D. J., & Stubbins, A. (2015). Chapter 8 - Marine Photochemistry of Organic

1122   Matter: Processes and Impacts. *Biogeochemistry of Marine Dissolved Organic Matter*

1123   *(Second Edition, eds.* D. A. Hansell & C. A. Carlson *)* (pp. 389–450). Academic Press.

1124   https://doi.org/10.1016/B978-0-12-405940-5.00008-X

1125 Orchard, E. D., Ammerman, J. W., Lomas, M. W., & Dyhrman, S. T. (2010). Dissolved inorganic

1126   and organic phosphorus uptake in Trichodesmium and the microbial community: The

1127   importance of phosphorus ester in the Sargasso Sea. *Limnology and Oceanography*,

1128   *55*(3), 1390–1399. https://doi.org/10.4319/lo.2010.55.3.1390

1129 Paulmier, A., & Ruiz-Pino, D. (2009). Oxygen minimum zones (OMZs) in the modern ocean.

1130   *Progress in Oceanography*, *80*(3), 113–128.

1131   https://doi.org/10.1016/j.pocean.2008.08.001

1132 Raymond, P. A., & Spencer, R. G. M. (2015). Chapter 11—Riverine DOM. *Biogeochemistry of*

1133   *Marine Dissolved Organic Matter (Second Edition, eds.* D. A. Hansell & C. A. Carlson*)* (pp.

1134   509–533). Academic Press. https://doi.org/10.1016/B978-0-12-405940-5.00011-X

1135   Redfield, A. C. (1934). On the proportions of organic derivations in seawater and their relation

1136   to the composition of plankton. *Univ. Press of Liverpool*, *James Johnstone memorial*

1137   *volume (ed. Daniel, R. J.)*, 177–192.

1138   Reynolds, S., Mahaffey, C., Roussenov, V., & Williams, R. G. (2014). Evidence for production and

1139   lateral transport of dissolved organic phosphorus in the eastern subtropical North

1140   Atlantic. *Global Biogeochemical Cycles*, *28*(8), 805–824.

1141   https://doi.org/10.1002/2013GB004801

1142   Roshan, S., & DeVries, T. (2017). Efficient dissolved organic carbon production and export in the

1143   oligotrophic ocean. *Nature Communications*, *8*(1), 2036.

1144   https://doi.org/10.1038/s41467-017-02227-3

1145   Siegel, D. A., DeVries, T., Cetinić, I., & Bisson, K. M. (2023). Quantifying the Ocean's Biological

1146   Pump and Its Carbon Cycle Impacts on Global Scales. *Annual Review of Marine Science*,

1147   *15*(1), 329–356. https://doi.org/10.1146/annurev-marine-040722-115226

1148   Singh, A., Baer, S. E., Riebesell, U., Martiny, A. C., & Lomas, M. W. (2015). C: N : P stoichiometry

1149   at the Bermuda Atlantic Time-series Study station in the North Atlantic Ocean.

1150   *Biogeosciences*, *12*(21), 6389–6403. https://doi.org/10.5194/bg-12-6389-2015

1151   Sipler, R. E., & Bronk, D. A. (2015). Chapter 4—Dynamics of Dissolved Organic Nitrogen.

1152   *Biogeochemistry of Marine Dissolved Organic Matter (Second Edition, eds.* D. A. Hansell

1153   & C. A. Carlson *)* (pp. 127–232). Academic Press. https://doi.org/10.1016/B978-0-12-

1154   405940-5.00004-2

1155   Sohm, J. A., & Capone, D. G. (2010). Zonal differences in phosphorus pools, turnover and

1156   deficiency across the tropical North Atlantic Ocean. *Global Biogeochemical Cycles*, *24*(2),

1157   GB2008. https://doi.org/10.1029/2008GB003414

1158   Stanley, R. H. R., Jenkins, W. J., Doney, S. C., & Lott III, D. E. (2015). The [3]He flux gauge in the

1159   Sargasso Sea: A determination of physical nutrient fluxes to the euphotic zone at the

1160   Bermuda Atlantic Time-series Site. *Biogeosciences*, *12*(17), 5199–5210.

1161   https://doi.org/10.5194/bg-12-5199-2015

1162   Tanioka, T., Larkin, A. A., Moreno, A. R., Brock, M. L., Fagan, A. J., Garcia, C. A., Garcia, N. S.,

1163   Gerace, S. D., Lee, J. A., Lomas, M. W., & Martiny, A. C. (2022). Global Ocean Particulate

1164   Organic Phosphorus, Carbon, Oxygen for Respiration, and Nitrogen (GO-POPCORN).

1165   *Scientific Data*, *9*(1), 688. https://doi.org/10.1038/s41597-022-01809-1

1166   Teng, Y.-C., Primeau, F. W., Moore, J. K., Lomas, M. W., & Martiny, A. C. (2014). Global-scale

1167   variations of the ratios of carbon to phosphorus in exported marine organic matter.

1168   *Nature Geoscience*, *7*(12), 895–898. https://doi.org/10.1038/ngeo2303

1169   Torres-Valdés, S., Roussenov, V. M., Sanders, R., Reynolds, S., Pan, X., Mather, R., Landolfi, A.,

1170   Wolff, G. A., Achterberg, E. P., & Williams, R. G. (2009). Distribution of dissolved organic

1171   nutrients and their effect on export production over the Atlantic Ocean. *Global*

1172   *Biogeochemical Cycles*, *23*(4). https://doi.org/10.1029/2008GB003389

1173   Trujillo-Ortiz, A., & Hernandez-Walls, R. (2021). *Gmregress: Geometric Mean Regression*

1174   *(Reduced Major Axis Regression. A MATLAB file.* http://www. mathworks.

1175   com/matlabcentral/fileexchange/27918-gmregress.

1176 Ustick, L. J., Larkin, A. A., Garcia, C. A., Garcia, N. S., Brock, M. L., Lee, J. A., Wiseman, N. A.,

1177   Moore, J. K., & Martiny, A. C. (2021). Metagenomic analysis reveals global-scale patterns

1178   of ocean nutrient limitation. *Science*, *372*(6539), 287–291.

1179   https://doi.org/10.1126/science.abe6301

1180 Van Mooy, B. A. S., Fredricks, H. F., Pedler, B. E., Dyhrman, S. T., Karl, D. M., Koblížek, M.,

1181   Lomas, M. W., Mincer, T. J., Moore, L. R., Moutin, T., Rappé, M. S., & Webb, E. A. (2009).

1182   Phytoplankton in the ocean use non-phosphorus lipids in response to phosphorus

1183   scarcity. *Nature*, *458*(7234), 69–72. https://doi.org/10.1038/nature07659

1184 Villareal, T. A., Altabet, M. A., & Culver-Rymsza, K. (1993). Nitrogen transport by vertically

1185   migrating diatom mats in the North Pacific Ocean. *Nature*, *363*(6431), 709–712.

1186   https://doi.org/10.1038/363709a0

1187 Wang, W.-L., Moore, J. K., Martiny, A. C., & Primeau, F. W. (2019). Convergent estimates of

1188   marine nitrogen fixation. *Nature*, *566*(7743), 205–211. https://doi.org/10.1038/s41586-

1189   019-0911-2

1190 Ward, B. B., Devol, A. H., Rich, J. J., Chang, B. X., Bulow, S. E., Naik, H., Pratihary, A., &

1191   Jayakumar, A. (2009). Denitrification as the dominant nitrogen loss process in the

1192   Arabian Sea. *Nature*, *461*(7260), 78–81. https://doi.org/10.1038/nature08276

1193 Westberry, T., Behrenfeld, M. J., Siegel, D. A., & Boss, E. (2008). Carbon-based primary

1194   productivity modeling with vertically resolved photoacclimation. *Global Biogeochemical*

1195   *Cycles*, *22*(2). https://doi.org/10.1029/2007GB003078

1196   Wirtz, K., Smith, S. L., Mathis, M., & Taucher, J. (2022). Vertically migrating phytoplankton fuel

1197   high oceanic primary production. *Nature Climate Change*, *12*(8), 750–756.

1198   https://doi.org/10.1038/s41558-022-01430-5

1199   Xu, H., & Weber, T. (2021). Ocean Dust Deposition Rates Constrained in a Data-Assimilation

1200   Model of the Marine Aluminum Cycle. *Global Biogeochemical Cycles*, *35*(9),

1201   e2021GB007049. https://doi.org/10.1029/2021GB007049

1202   Zehr, J. P., & Ward, B. B. (2002). Nitrogen Cycling in the Ocean: New Perspectives on Processes

1203   and Paradigms. *Applied and Environmental Microbiology*, *68*(3), 1015–1024.

1204   https://doi.org/10.1128/AEM.68.3.1015-1024.2002

1205   Zhang, R., Wang, X. T., Ren, H., Huang, J., Chen, M., & Sigman, D. M. (2020a). Dissolved Organic

1206   Nitrogen Cycling in the South China Sea From an Isotopic Perspective. *Global*

1207   *Biogeochemical Cycles*, *34*(12), e2020GB006551.

1208   https://doi.org/10.1029/2020GB006551

1209   Zhang, X., Ward, B. B., & Sigman, D. M. (2020b). Global Nitrogen Cycle: Critical Enzymes,

1210   Organisms, and Processes for Nitrogen Budgets and Dynamics. *Chemical Reviews*,

1211   *120*(12), 5308–5351. https://doi.org/10.1021/acs.chemrev.9b00613

1212   Zhang, Y., Mahowald, N., Scanza, R. A., Journet, E., Desboeufs, K., Albani, S., Kok, J. F., Zhuang,

1213   G., Chen, Y., Cohen, D. D., Paytan, A., Patey, M. D., Achterberg, E. P., Engelbrecht, J. P., &

1214   Fomba, K. W. (2015). Modeling the global emission, transport and deposition of trace

1215   elements associated with mineral dust. *Biogeosciences*, *12*(19), 5771–5792.

1216   https://doi.org/10.5194/bg-12-5771-2015

1217
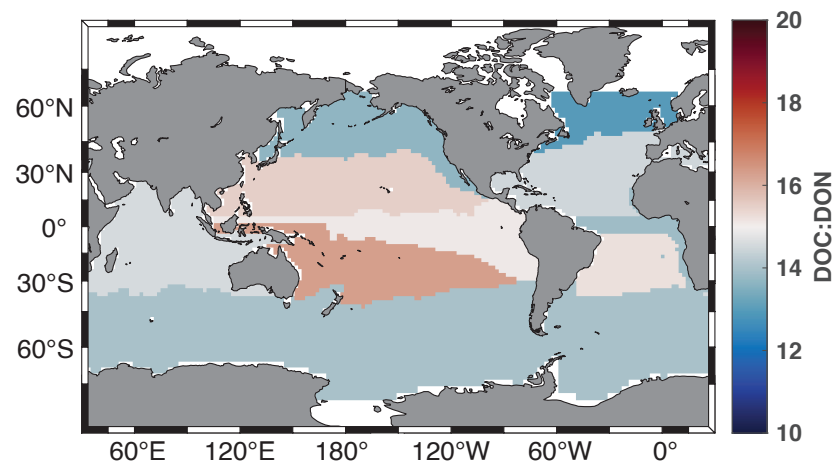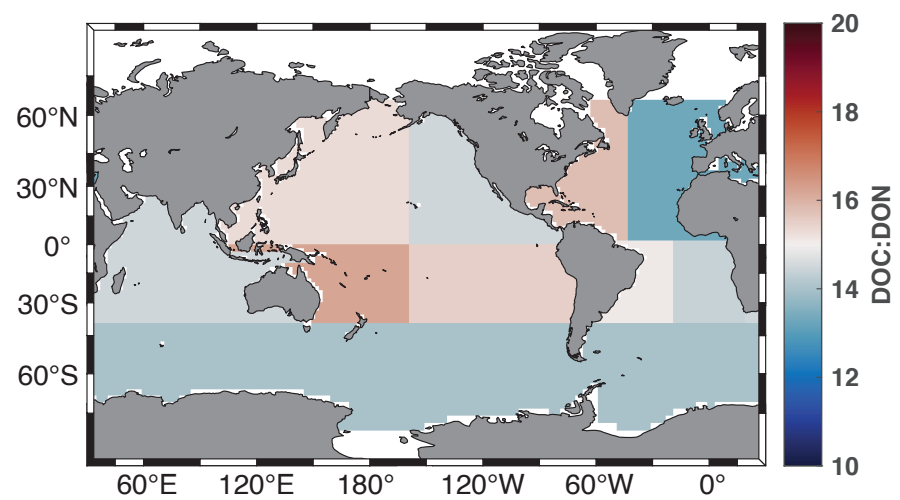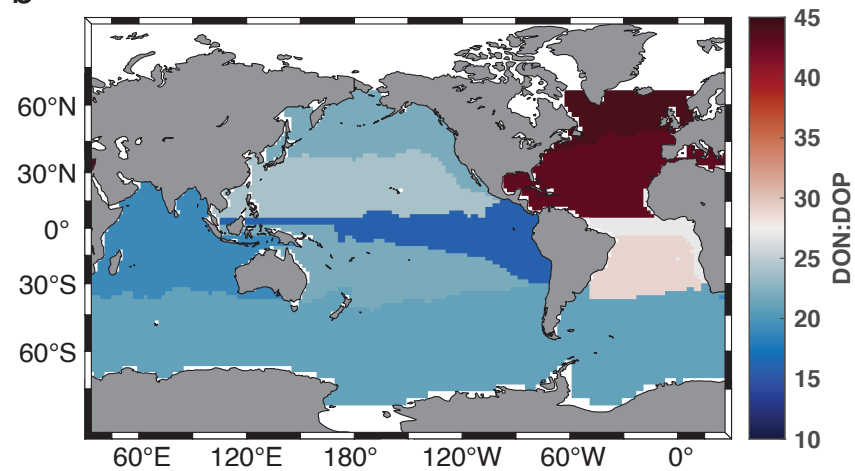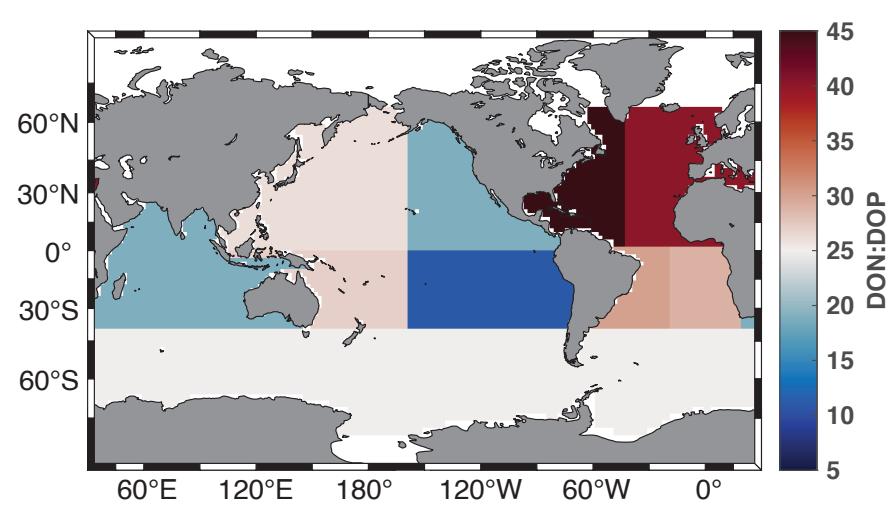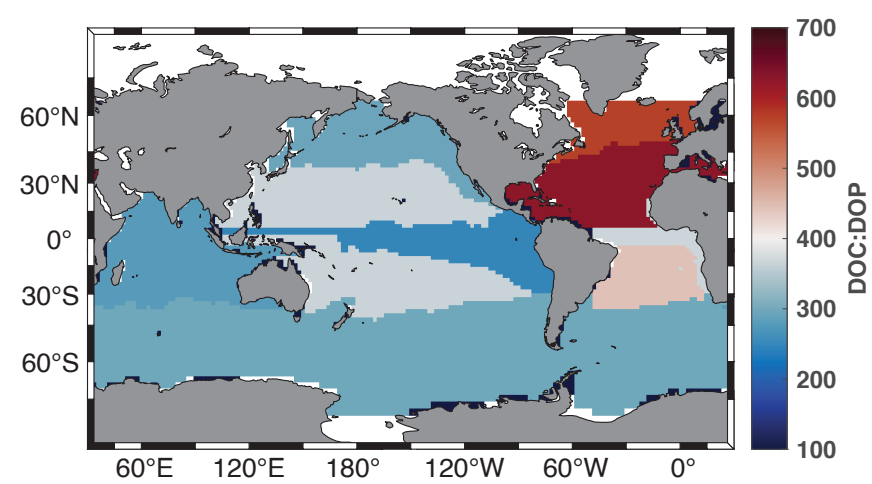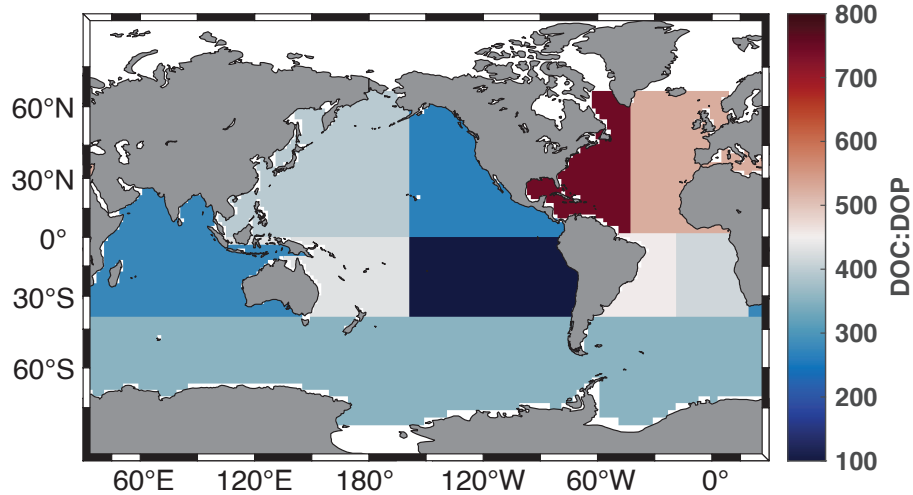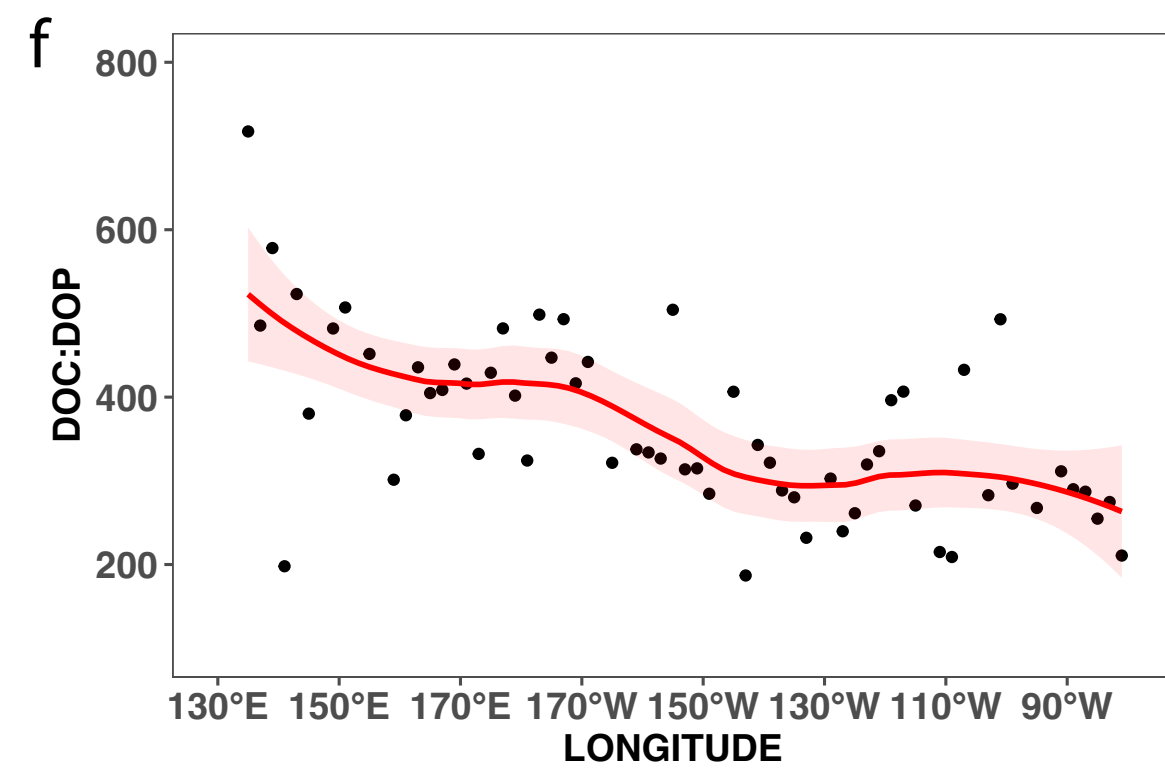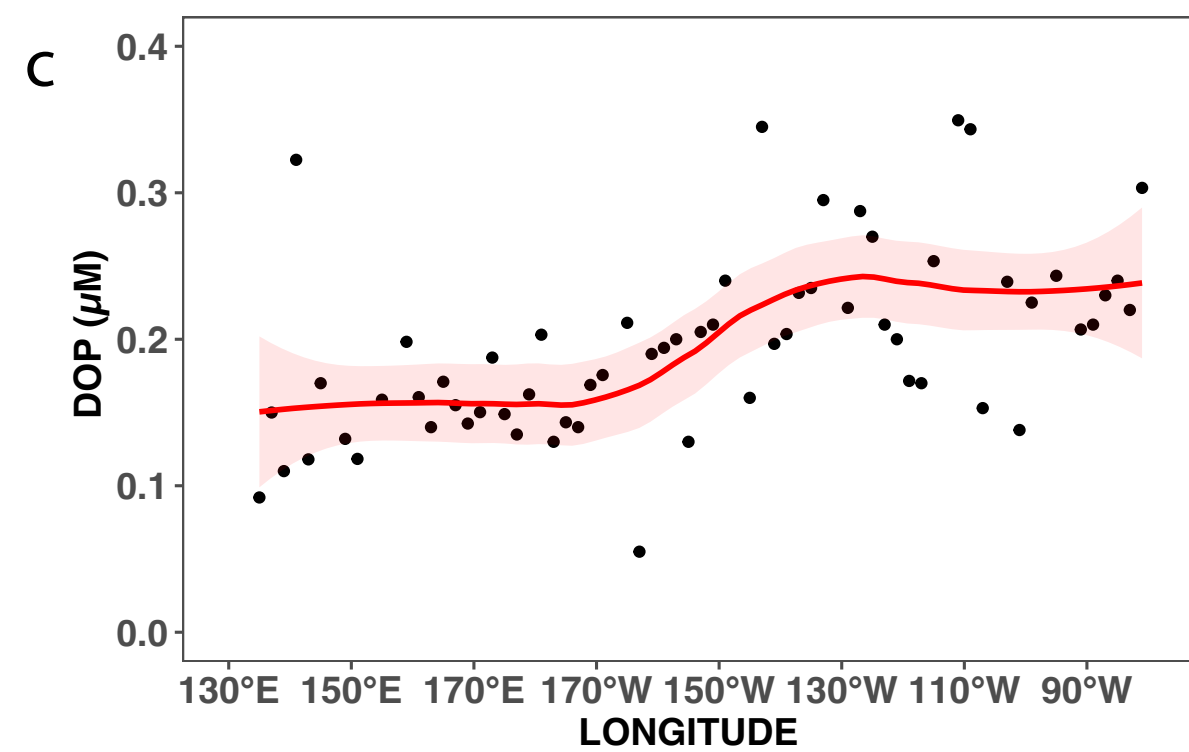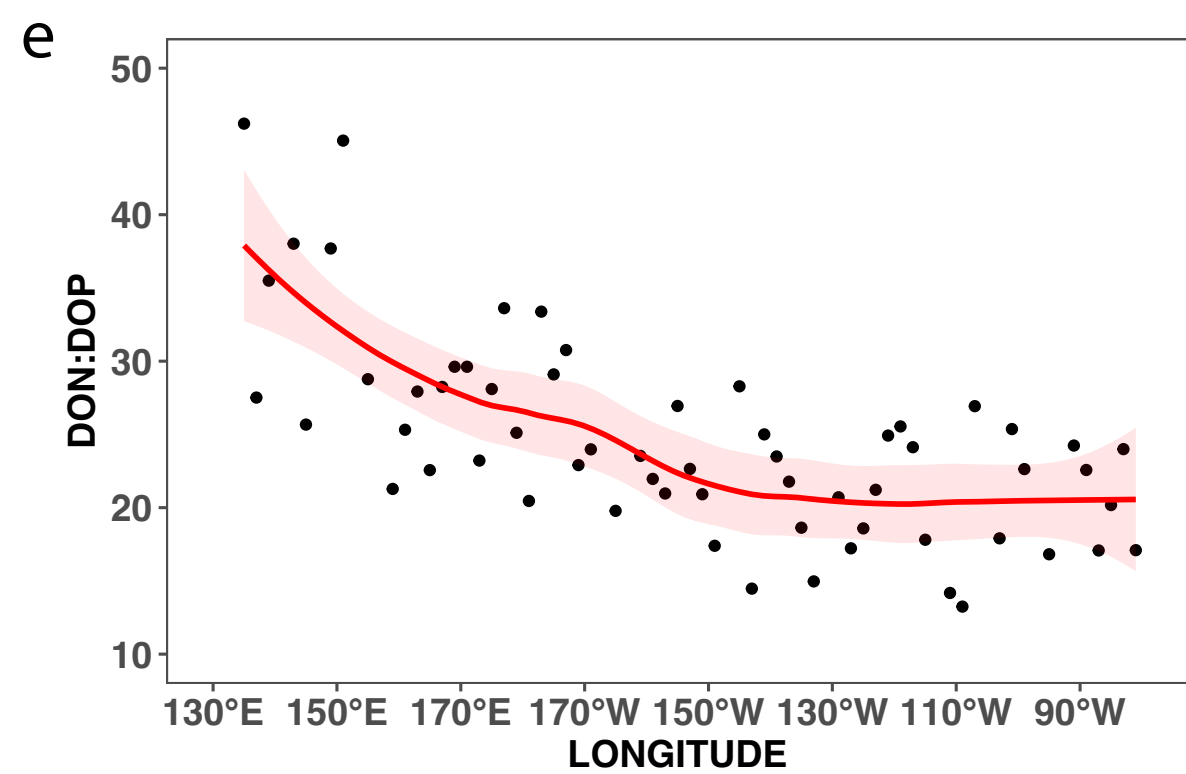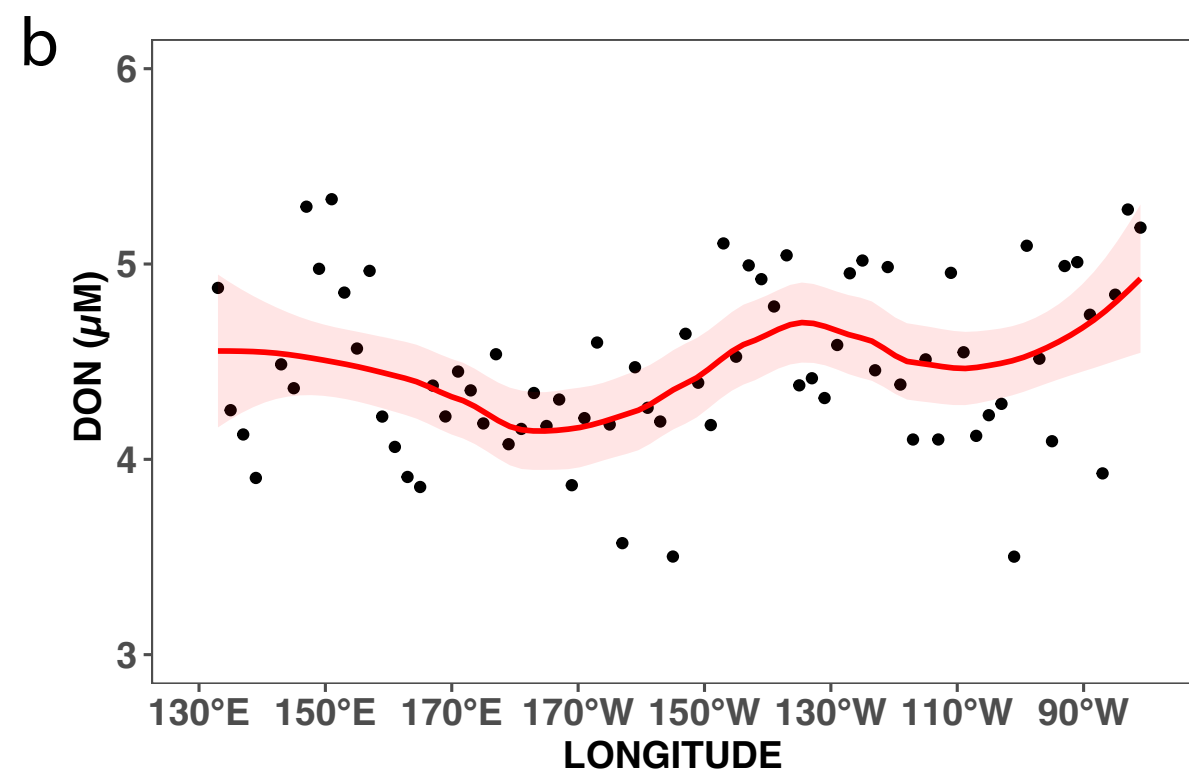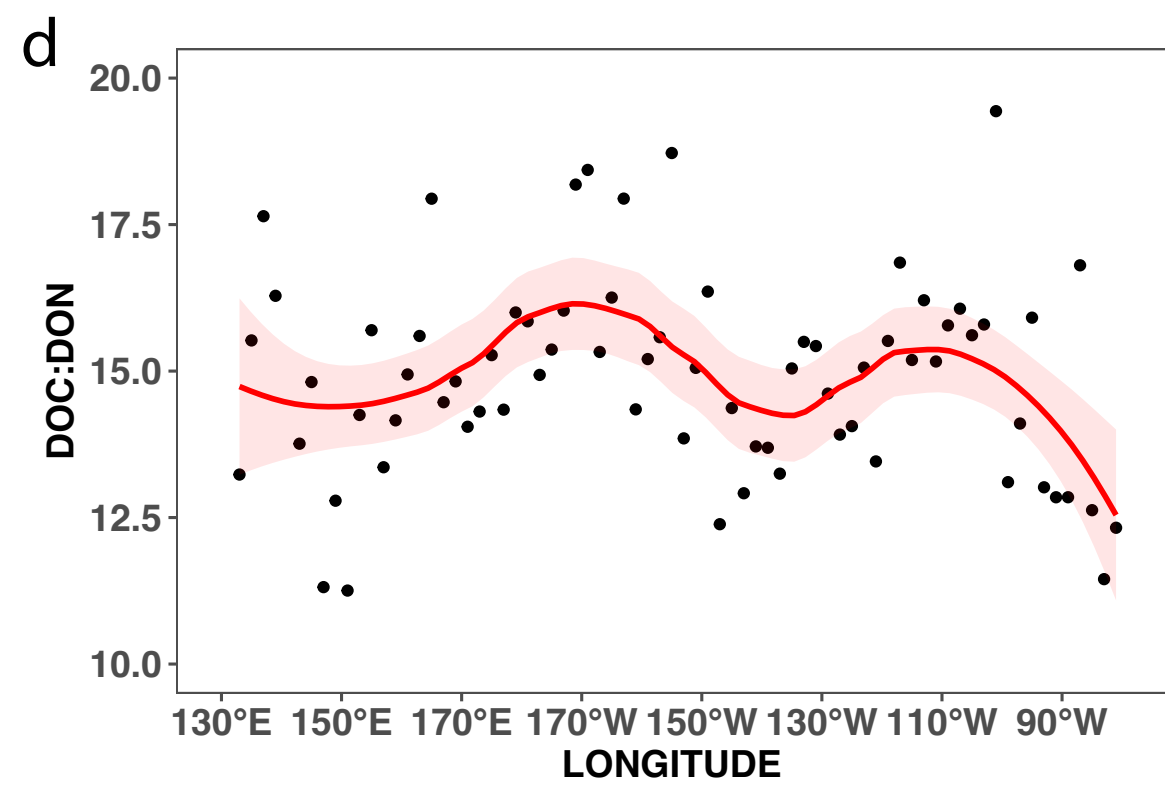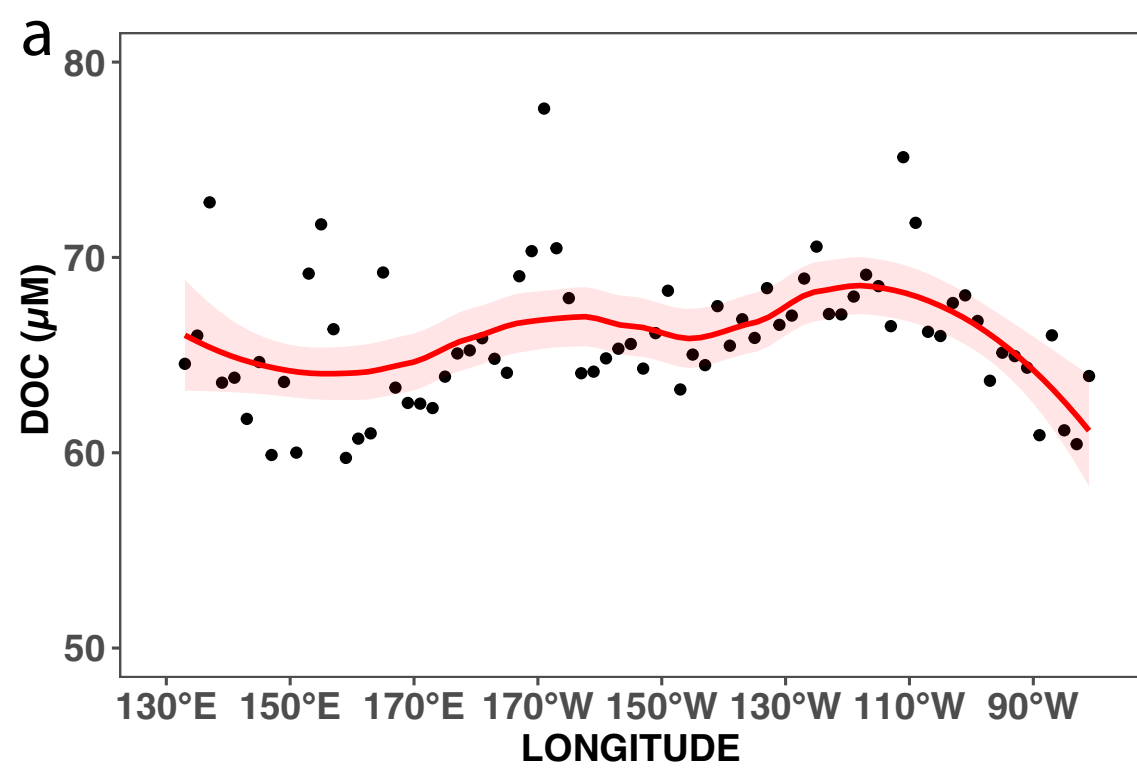
Figure 1.
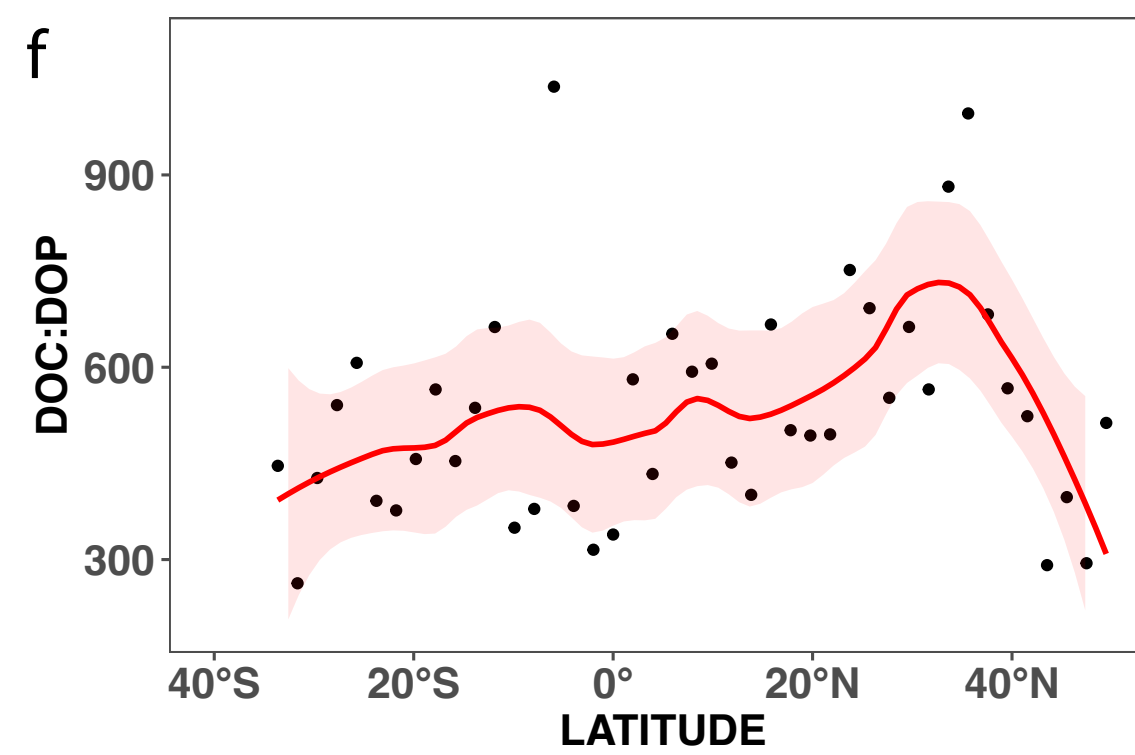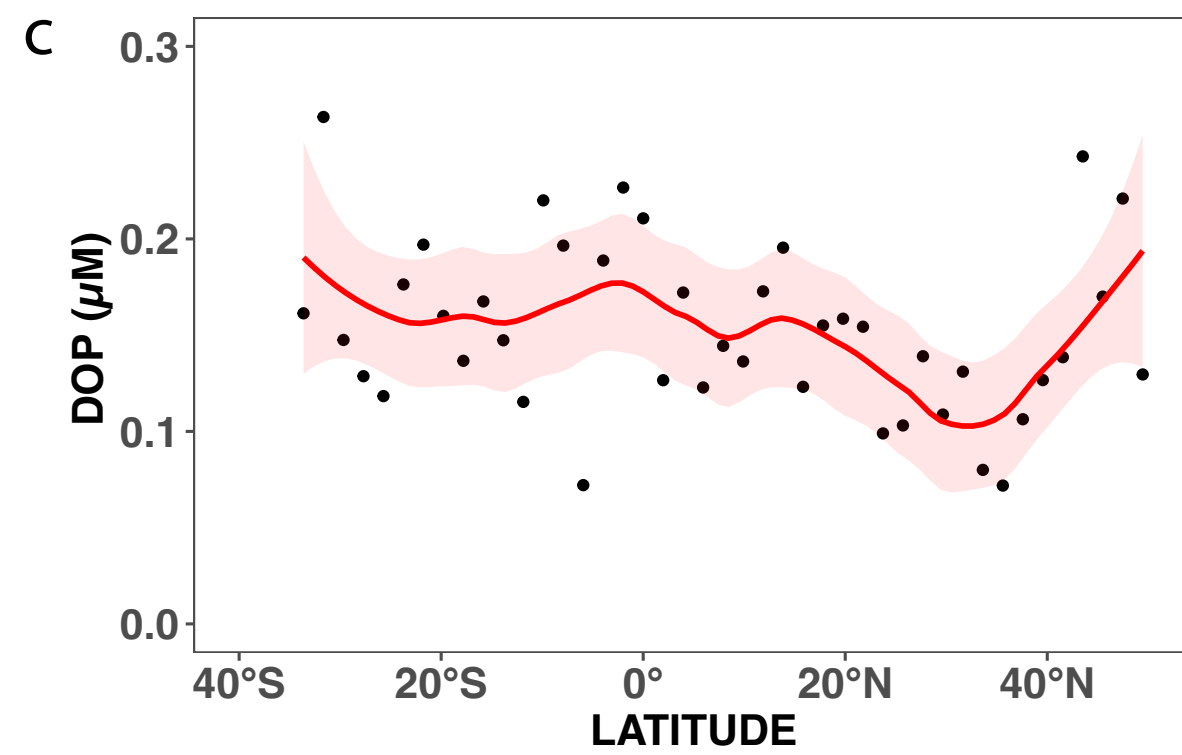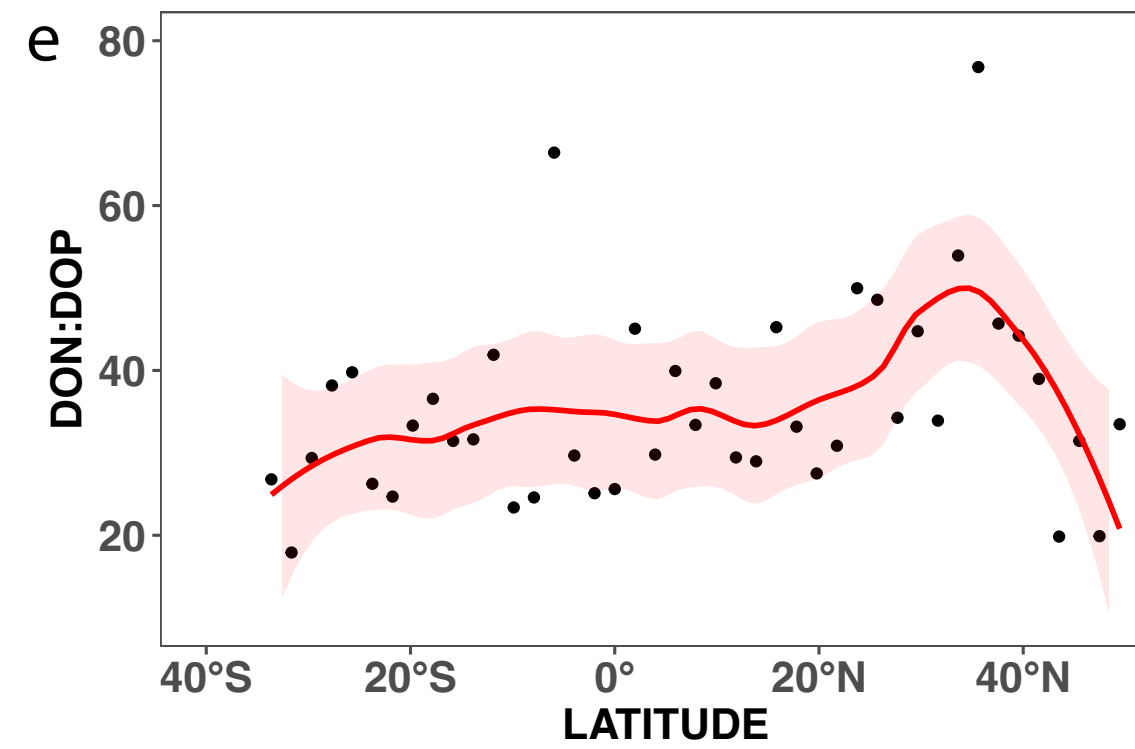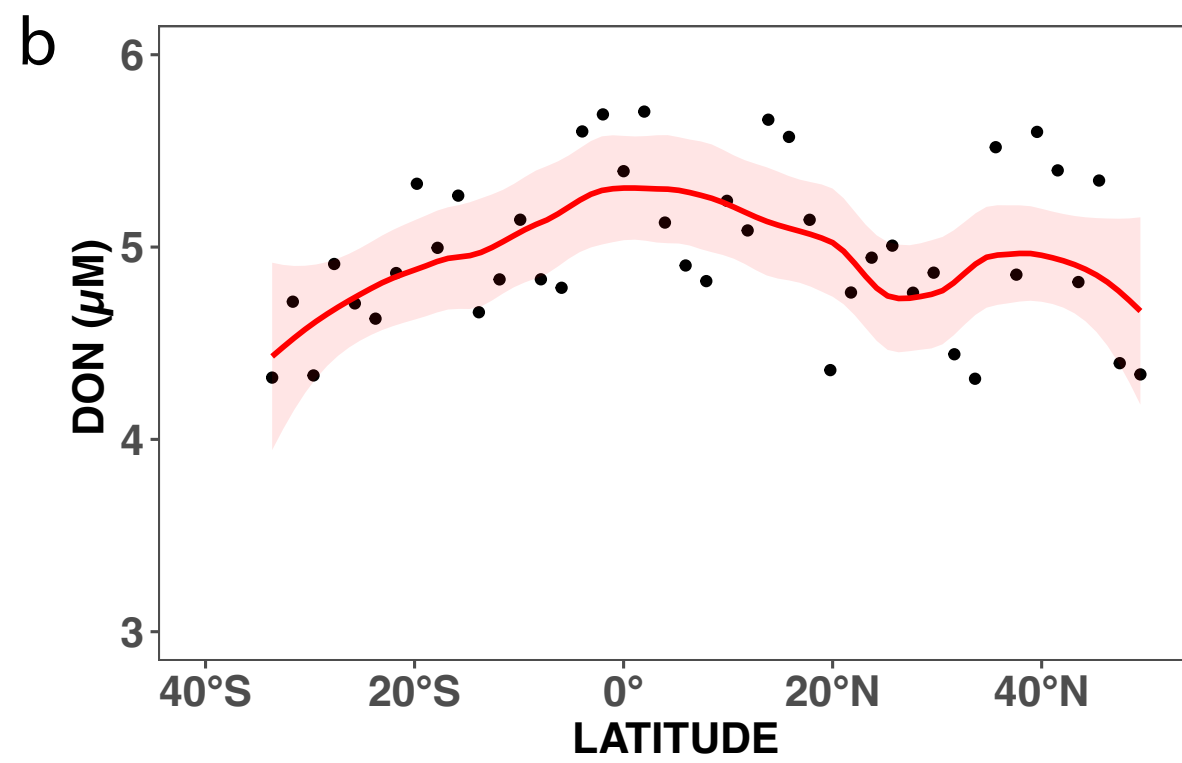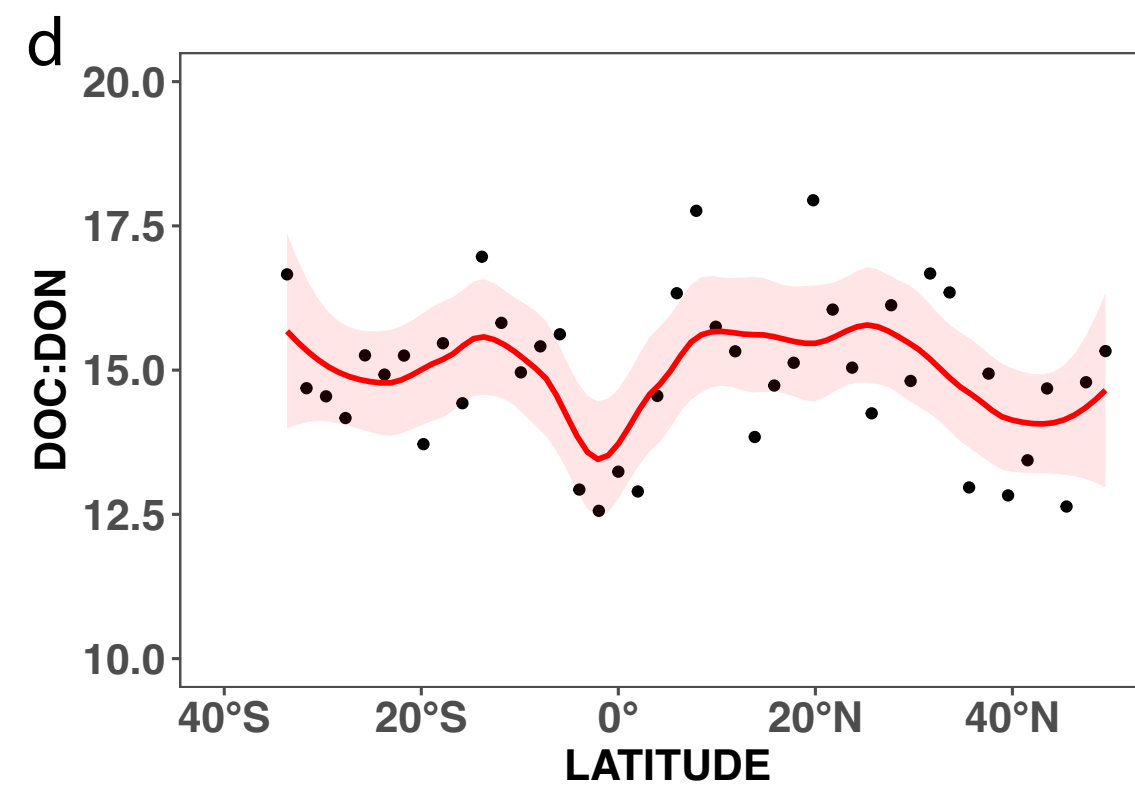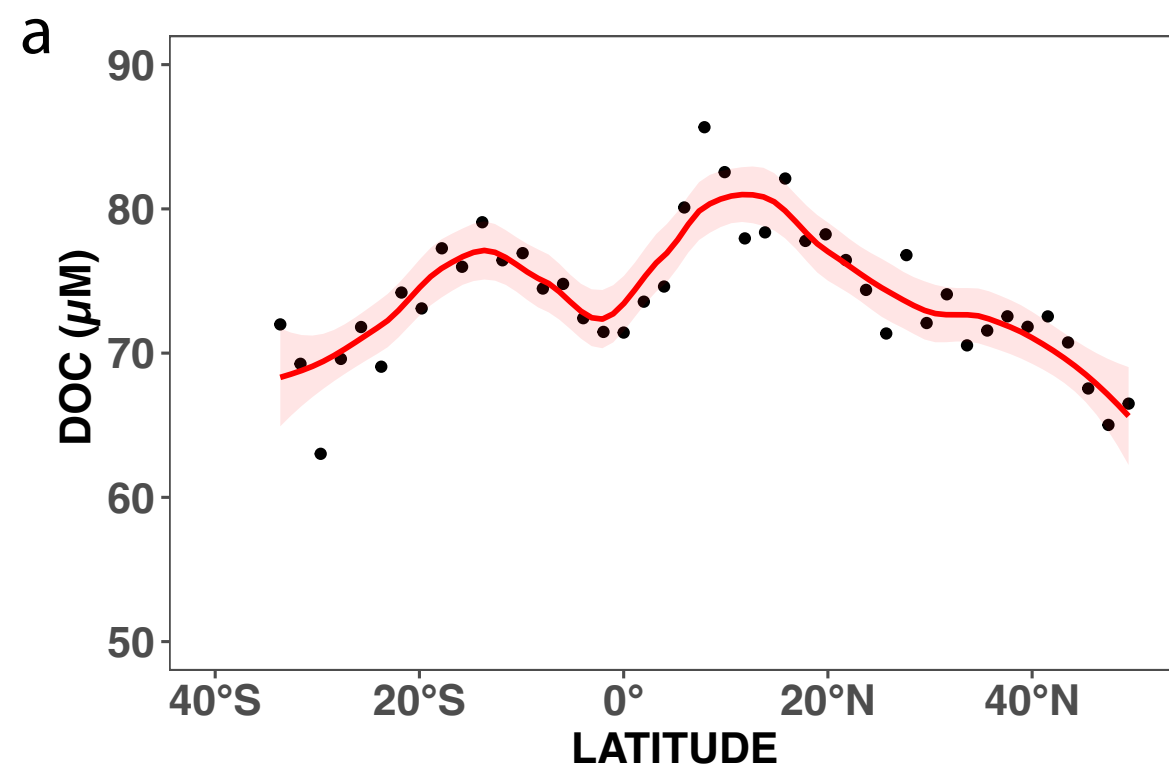
Figure 2.

Figure 3.

Figure 4.

a
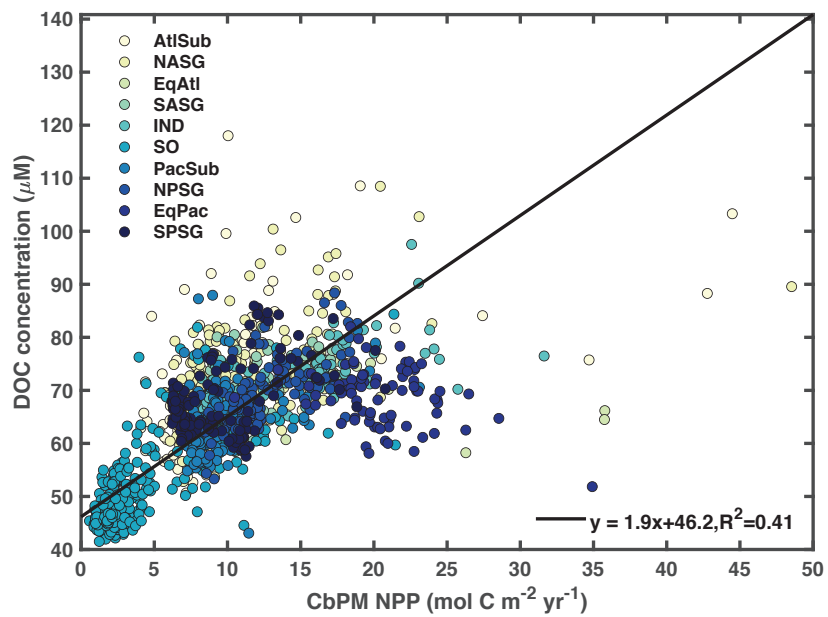
b

c
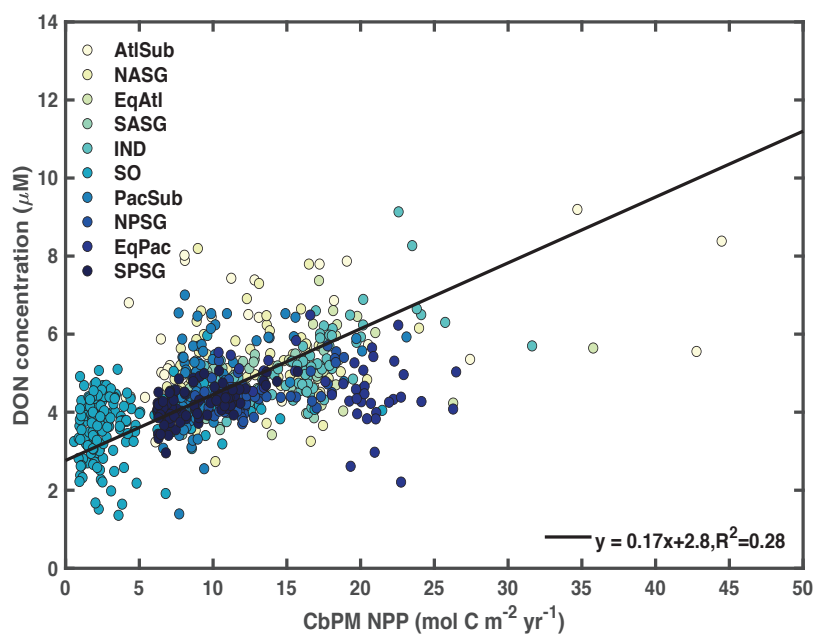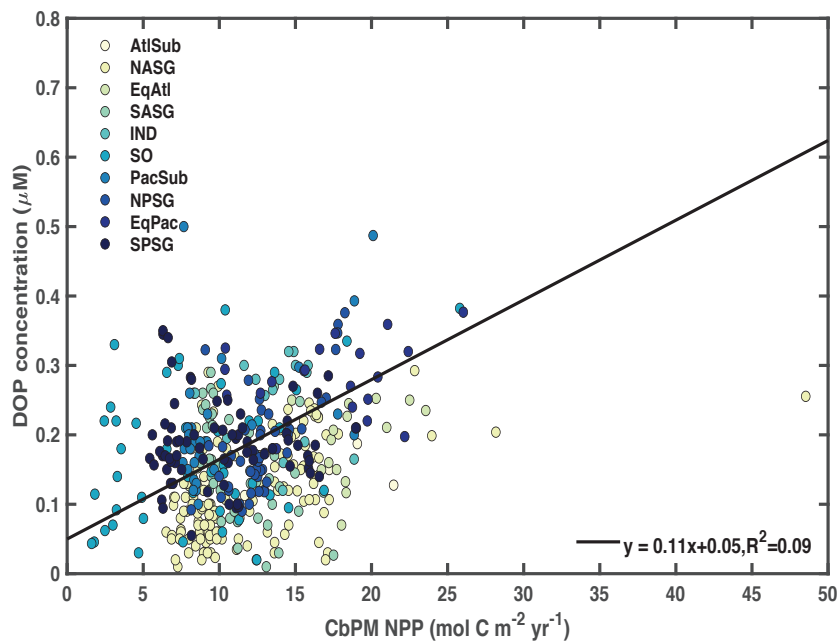
Figure 5.
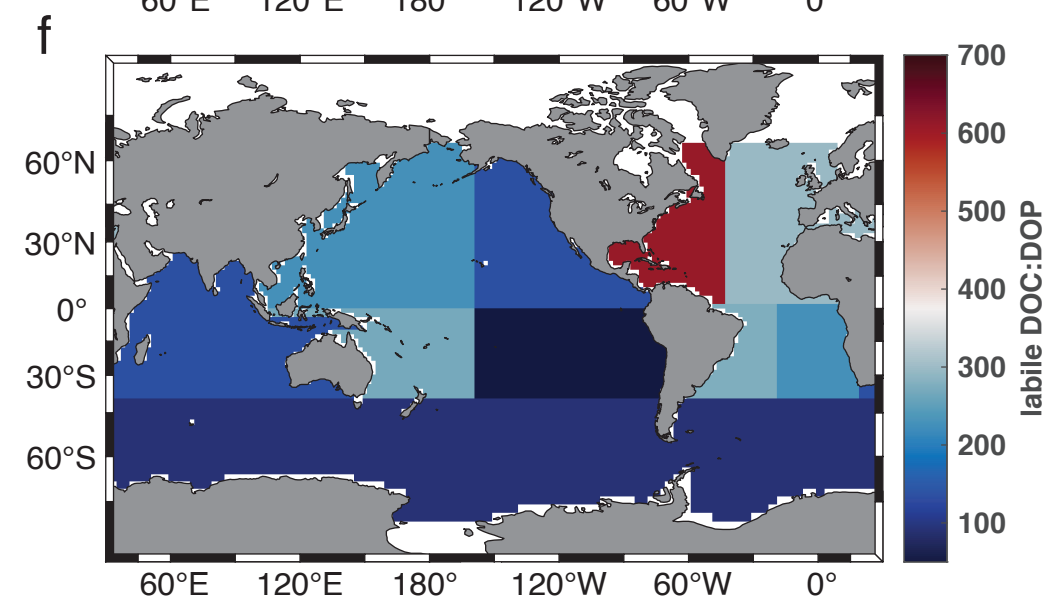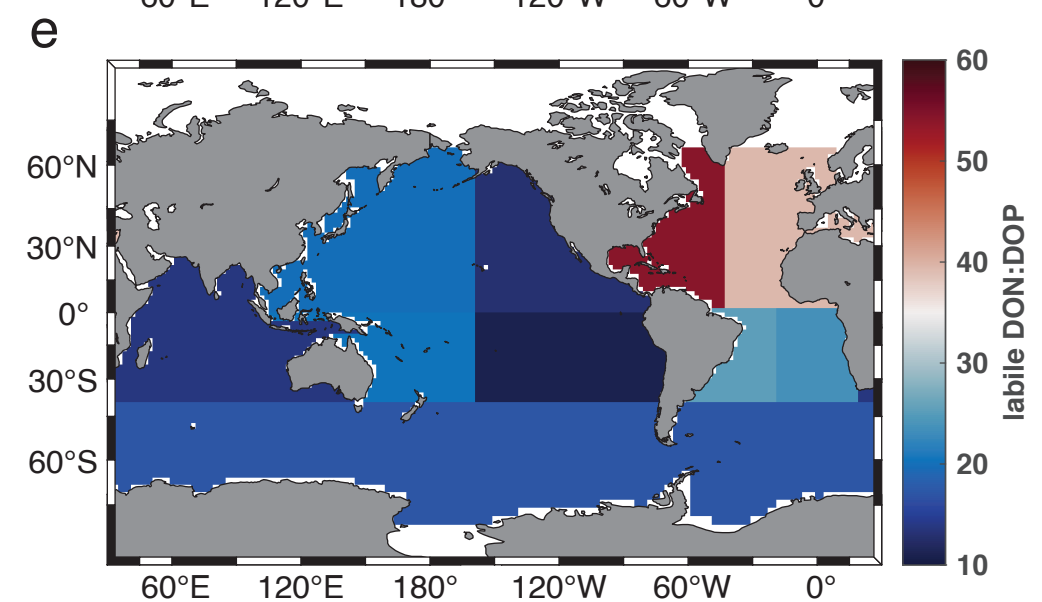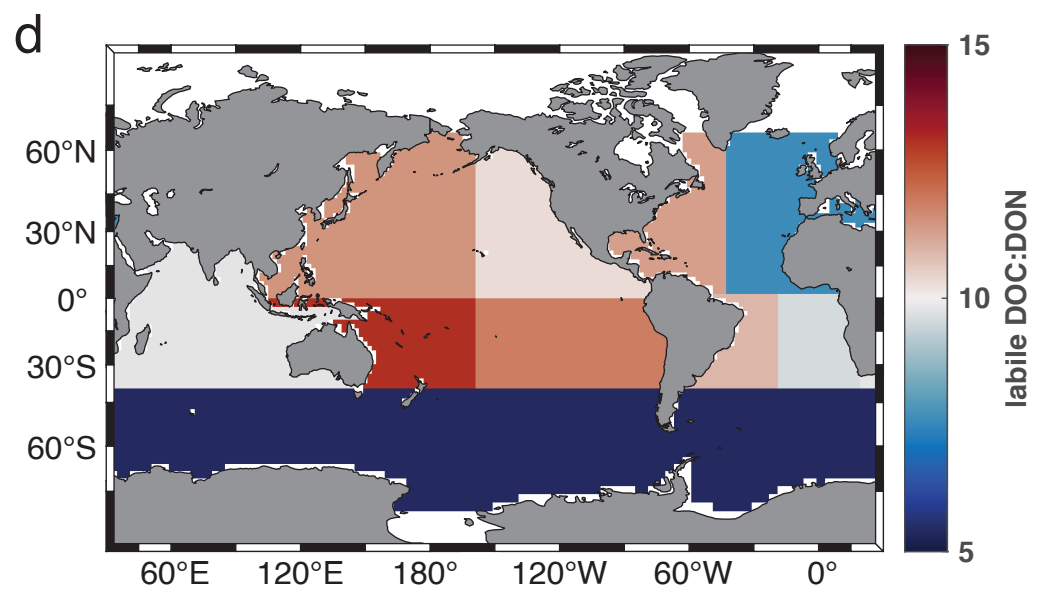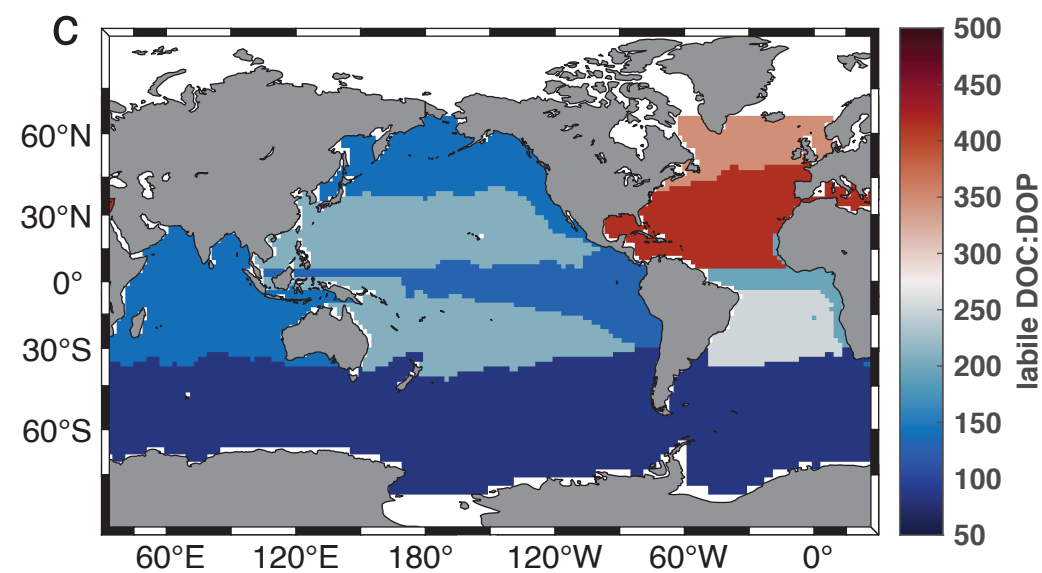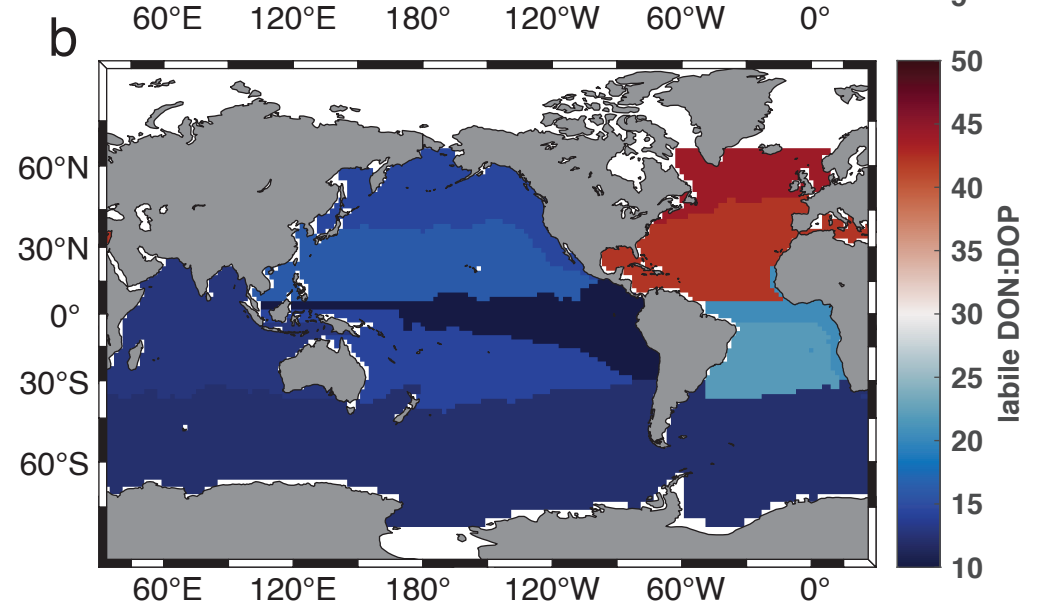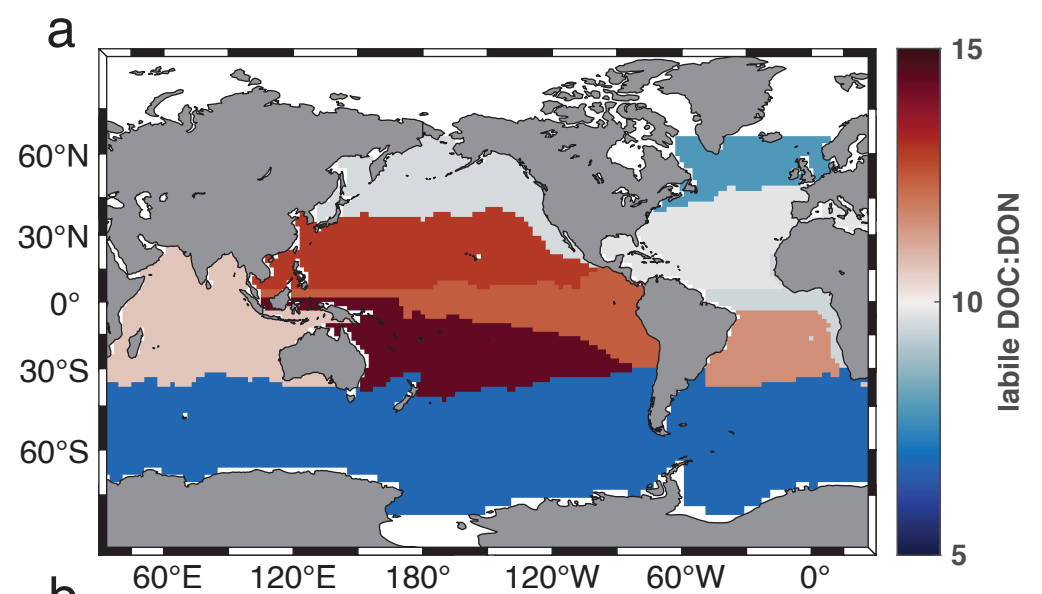
Figure 6.
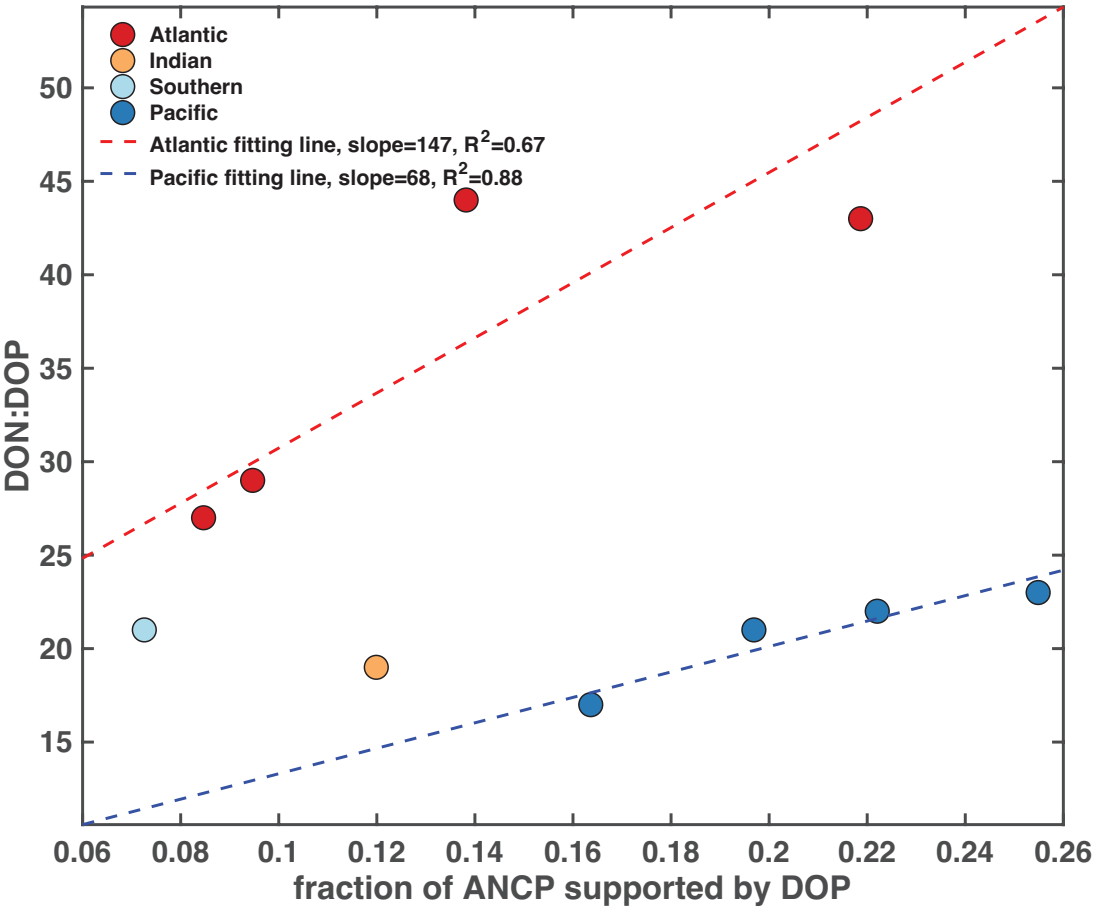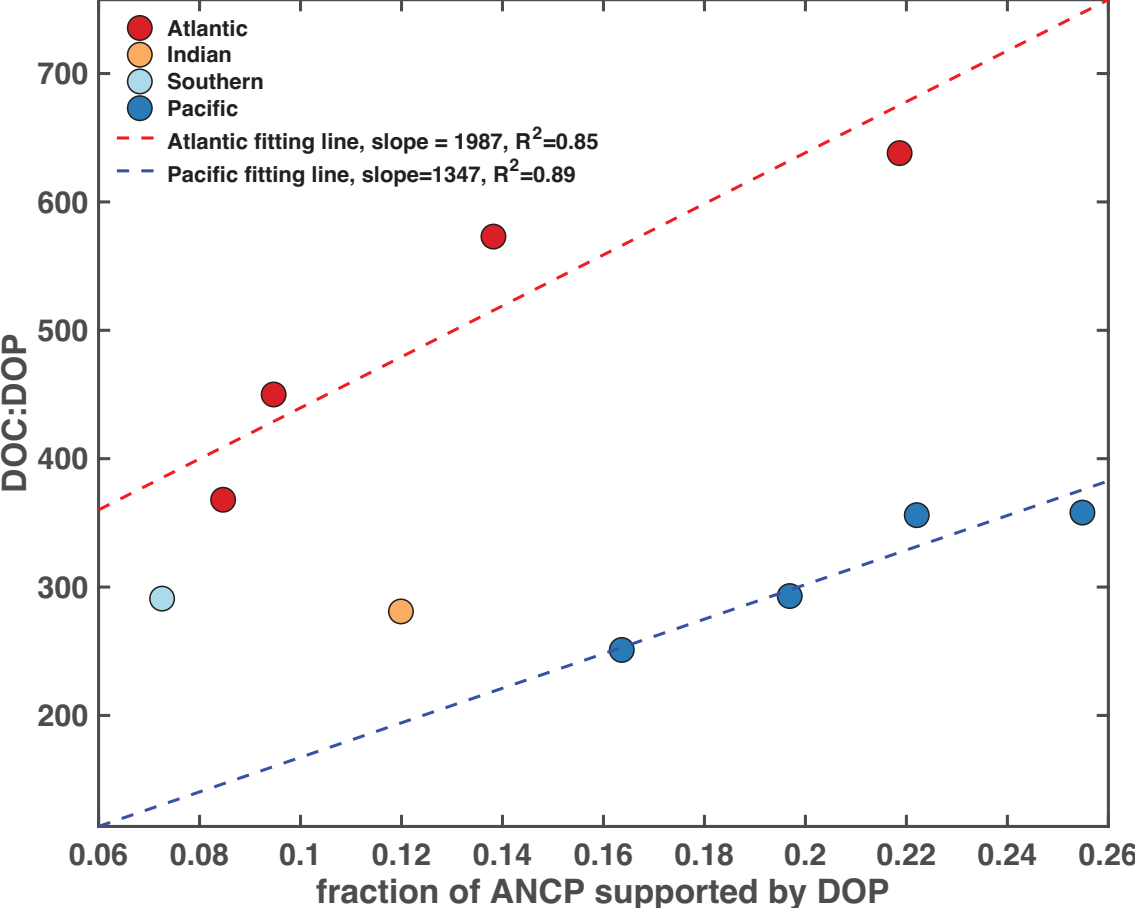
Figure 7.

Figure 8.

Figure 9.